5G Scheduling for Distributed Control in Microgrids

Rahul R Iyer

Thesis submitted to the Faculty of the
Virginia Polytechnic Institute and State University
in partial fulfillment of the requirements for the degree of

Master of Science
in
Electrical Engineering

Ali Mehrizi-Sani, Chair
Vijay Shah
Chen-Ching Liu

October 8th, 2021
Blacksburg, Virginia

Keywords: Age of information, distributed control, distributed energy resources, microgrids, scheduling, 5G

5G Scheduling for Distributed Control in Microgrids

Rahul R Iyer

ABSTRACT

There is an increasing integration of distributed energy resources (DER), controllable loads, and other technologies that are making the grid more robust, reliable, and decentralized. Communication is a major aspect that enables this decentralization and can improve control of important system parameters by allowing different grid components to communicate their states with each other. This information exchange requires a reliable and fast communication infrastructure. Different communication techniques can be used towards this objective, but with recent technological advancements, 5G communication is proving to be a very viable option. 5G is being widely deployed throughout the world due to its high data rates combined with increased reliability compared with its predecessor technologies. This thesis focuses on application and performance analysis of a 5G network for different power system test cases. These test cases are microgrids, and consist of DERs that use distributed control for efficient operation. Under distributed control, the DERs communicate with each other to achieve fast and improved dynamic response. This work develops a co-simulation platform to analyze the impact that a 5G network has in this distributed control objective. This offers key insights on 5G's capability to support critical functions. Different scenarios including set point changes and transients are evaluated. Since distributed control is a time-critical application and DERs rely on the availability of up-to-date information, the scheduling aspect of 5G becomes very important and is given more focus. Information freshness measured using age of information (AoI) is used in this work. Information freshness is a measure of how recent and updated the information communicated by DERs is. This thesis compares the performance of AoI-based schedulers against standard schedulers. These different schedulers are then used on test systems employing distributed control.

5G Scheduling for Distributed Control in Microgrids

Rahul R Iyer

GENERAL AUDIENCE ABSTRACT

Communication has become an important aspect of modern power systems due to increased integration of distributed energy resources (DER), controllable loads and other components that have communication capabilities for improved grid performance. Of the various communication techniques available for power systems, 5G is very promising due to its advantages over its predecessors and other wired communication methods. This work develops a co-simulation framework to implement a 5G network for different microgrid test cases that employ distributed control. Under distributed control, the DERs communicate with each other to achieve fast and improved dynamic response. Due to the time-critical nature of distributed control, DERs rely on the availability of up-to-date information. Hence the scheduling aspect of 5G becomes very important and is given more focus in this work. 5G schedulers that account for the availability of up-to-date information, also referred to as information freshness, are compared with standard 5G schedulers and their performance in distributed control test systems is analyzed.

Dedication

This work is dedicated to my amma (mother) and appa (father)

Contents

List of Figures

List of Tables

Chapter 1

Introduction

The U.S. Department of Energy (DOE) defines a microgrid as ‘‘a group of interconnected loads and distributed energy resources (DERs) within clearly defined electrical boundaries that acts as a single controllable entity with respect to the grid. A microgrid can connect and disconnect from the grid to enable it to operate in both grid-connected or island-mode [4].” The microgrid is connected to the main grid through a point of common coupling (PCC). A microgrid can have different elements and different topologies, but a generic microgrid structure and its elements is showed in Fig. 1.1.

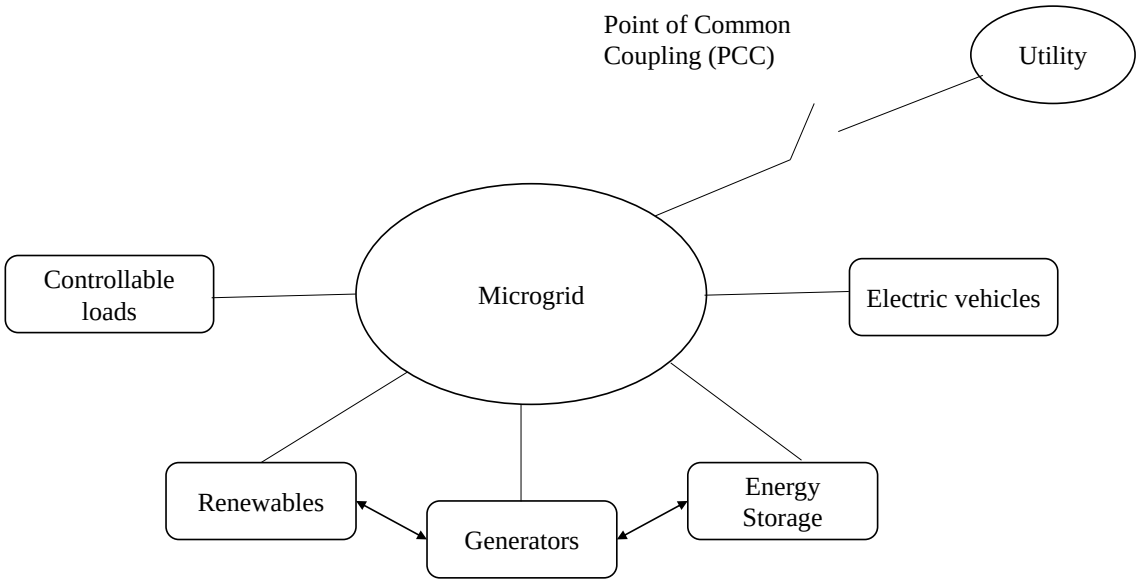

Figure 1.1: Generic structure and elements in a microgrid.

Following are the advantages of microgrids over the conventional grid [5]:

1. Integration of DERs in microgrids leads to less consumption of carbon and reduces energy costs.
2. Transmission losses are reduced due to the proximity of generation and load compared to the traditional grid. Hence microgrids are more energy efficient.
3. Microgrids offer faster demand response compared to conventional grid.
4. Since DERs are integrated with inverters, there is better voltage regulation and power quality increases.

1.1 AC Microgrids

AC microgrids consist of generation sources and loads that are connected through an AC bus system [6]. The generation sources can include renewable energy sources as well as conventional sources like engine-based generators. If there are renewable energy sources like photo-voltaic cells or battery energy systems, they are first converted to AC through power electronic based inverters before connecting to the AC microgrid network.

Following are the advantages of an AC microgrid [6]:

1. Easy integration with the conventional utility grid.
2. No inverter requirement for AC loads.
3. Cost efficient in power protection systems.

Following are the disadvantages of an AC microgrid [6]:

1. Conversion efficiency for power generated by PV cells or battery systems is low.
2. High cost requirement due to inverters for DC to AC conversion.
3. Lower transmission efficiency compared to DC microgrids.

1.2 Levels of Control

1.2.1 Primary Control

Primary control is the first level of control and has the fastest response among the differnt control levels. The response time is typically in milliseconds. Fundamental electrical quantities like voltage and frequency are controlled at this level. Islanding detection and associated change in controller modes can also be implemented at this level [7]. This layer typically provides inverter output control and power sharing control [8]. Inverter output control typically employs an inner loop that controls current and an outer loop that controls voltage. Different frames of reference including synchronous (dq), stationary ($\alpha\beta$), and natural (abc) can be employed for inverter output control [9].

Primary control can also be broadly classified as follows:

1. Droop based control
2. Non-droop/communication based control [8].

Droop Based Control

The conventional $P - f/Q - V$ droop control stems from the droop characteristics of a synchronous generator. Voltage and frequency are the control variables. The advantages of

this method are that it provides flexibility, redundancy and easy implementation. Drawbacks include slow transient response, inaccurate power sharing, and circulating currents.

Non-Droop/Communication Based Control

These methods include a centralized control scheme [10], master/slave based approach [11] or a distributed control scheme [12]. Communication between the individual DER units ensures accurate power sharing, good power quality, and good transient response. However, this comes at a price of implementing communication. Scalability also becomes an issue if long range communication is involved.

1.2.2 Secondary Control

Secondary control aims to serve objectives like voltage profile control, power quality control, reactive power sharing, and loss reduction [13]. It also facilitates synchronization with the main grid. Since it ensures reliable and economical operation of microgrids, it is also referred to as the microgrid energy management system (EMS). It generally operates at a slower time frame and has a settling time of around a minute to decouple it from primary control [14]. Secondary control can be implemented using centralized [15] and decentralized methods [16]. Centralized control method is used when the microgrid has a relatively fixed structure since it is not preferred in cases requiring plug-and-play. On the other hand, decentralized control is preferred for grid-connected microgrids with variable number of DERs.

1.2.3 Tertiary Control

Tertiary control is the outermost and slowest level of control in microgrids. It is concerned with global responsibilities like import and exchange of power for the microgrid in a system with multiple microgrids [17]. It is also used to regulate the power flow between the microgrid and the main grid at the point of common coupling (PCC).

1.3 Control Strategies

1.3.1 Centralized Control

Centralized control in a microgrid is implemented with the help of a central controller and a communication network. Local controller present at individual DERs are used to control are used for individual DER control. The electrical parameters that need to be controlled globally, e.g., voltage at PCC or frequency, are controlled by the central controller. The central controller provides the necessary control signals to the local controllers. Fig.1.2 shows the centralized control scheme. In a grid connected microgrid, the central controller also performs the task of exchanging reactive power with the main grid [18].

A centralized control scheme in microgrids has many applications. A robust centralized control scheme for DC islanded microgrids is developed in [19]. Reference [20] discusses a multistage centralized control scheme for islanded microgrids with plug-in electric vehicles. Reference [21] proposes a centralized architecture for islanded AC microgrids with DERs and energy storage units. Centralized control strategies for grid connected microgrids are discussed in [22] and [23]. However, this control scheme also suffers from a few drawbacks [13]. These are enumerated below:

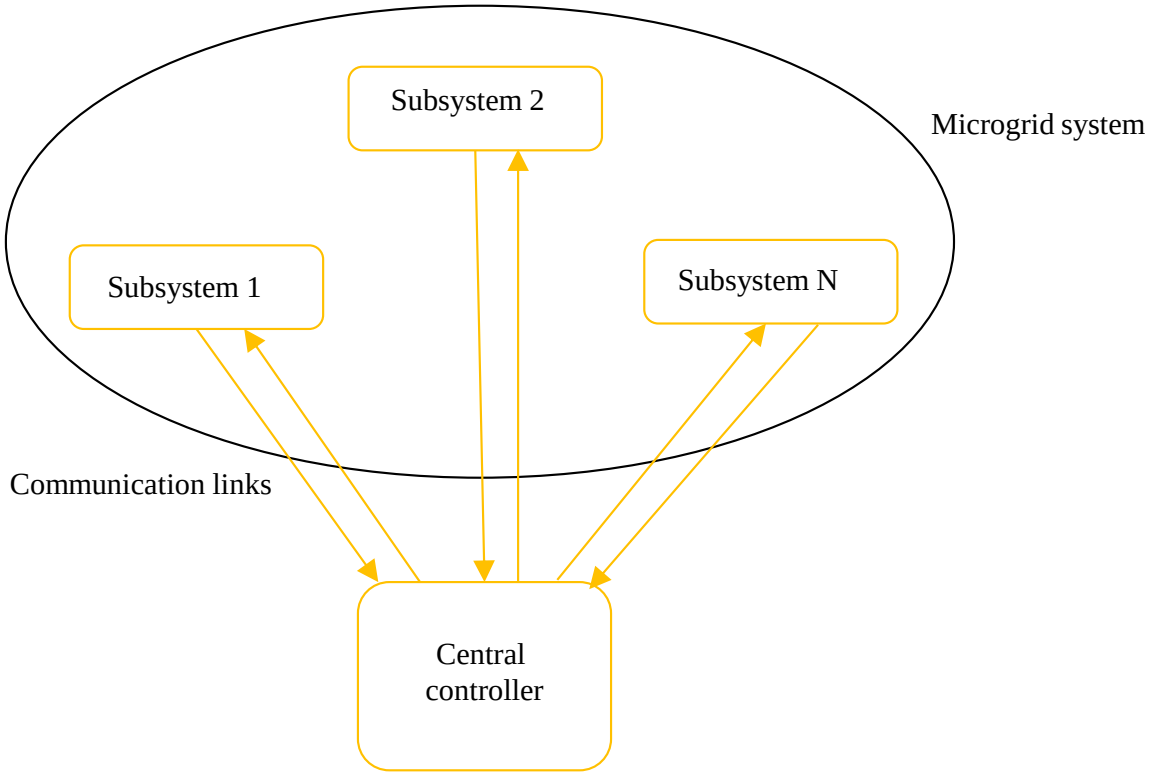

Figure 1.2: Centralized control approach. Subsystem may include individual or a group of DERs or controllable loads.

1. There is a single point of failure in a centralized control scheme.

2. Plug-and-play operation of DERs becomes difficult due to increased control and computational burden on the central controller.

3. Depending on topology and span, communication requirements and costs can be very high.

1.3.2 Decentralized Control

In the decentralized control approach, the microgrid is divided into subsystems and a local controller is assigned to each subsystem. When designing each local controller, interactions

from other subsystems is ignored [24]. Fig. 1.3 shows the decentralized scheme. Only information availbale locally within each subsystem is used for the controller design. Hence there is a restriction in terms of the control area which causes performance deterioration. The widespread blackout of August 2003 is an example of the failure of the decentralized control approach [25]. In this event, a cascading failure occurred because each subsystem focused on maintaining its own stability and transferred the extra load to the other subsystems. This increased the severity of the overload and ultimately resulted in a blackout.

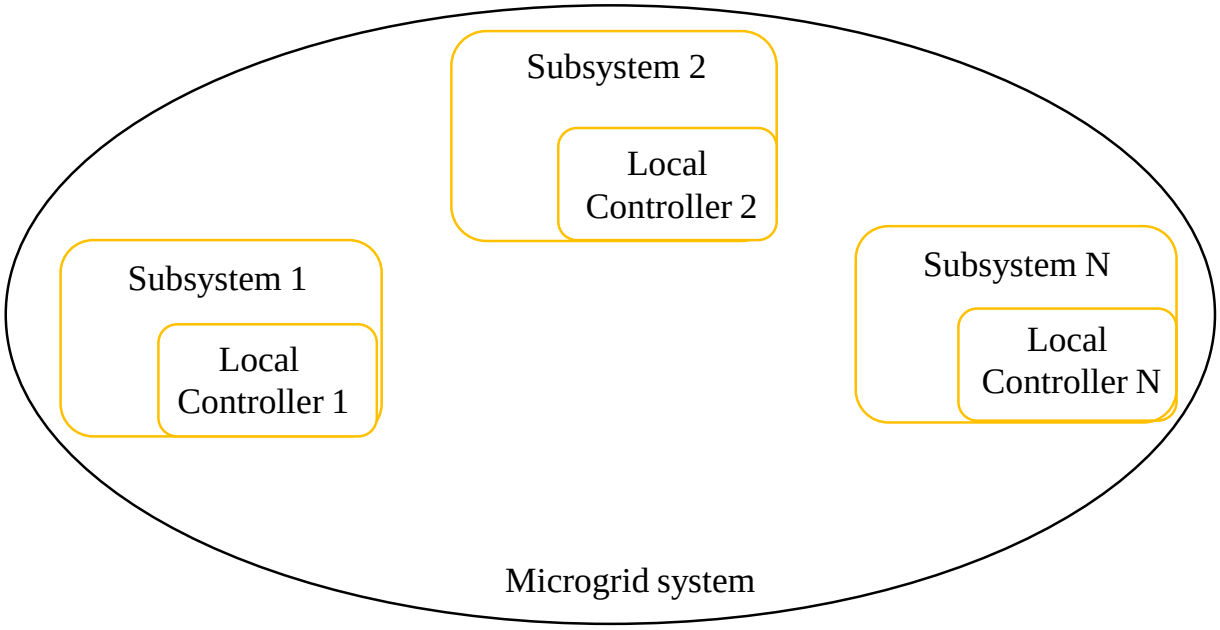

Figure 1.3: Decentralized control approach. Subsystem may include individual or a group of DERs or controllable loads.

The system control performance would improve if the decentralized local controllers exchanged information over a communication network. This leads to the distributed control approach which is discussed next.

1.3.3 Distributed Control

Distributed control methods are advantageous because they combine the benefits of centralized and decentralized methods. Under distributed control, DERs interact with each other for better coordination and performance [13]. Local DER measurements (e.g., voltage, current, real/reactive power, and frequency) are communicated to neighboring DERs. The distributed control scheme is shown in Fig. 1.4. The information may be exchanged with all neighboring DERs [26], or only select DERs [27] to reduce the communication burden. Distributed control techniques can be applied at different levels of control, although typically they are used in the secondary [28] and tertiary levels [29].

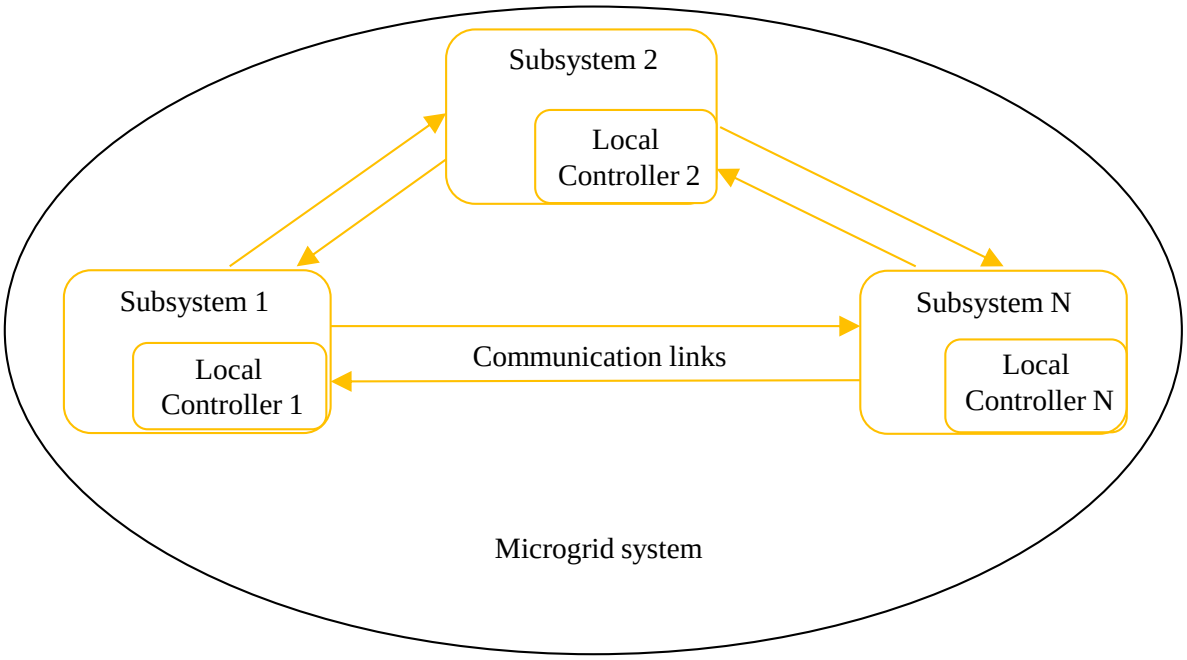

Figure 1.4: Distributed control approach. Subsystem may include individual or a group of DERs or controllable loads.

There are many applications of distributed control in microgrids. It's application in islanded AC microgrids is discussed in [30]. Distributed cooperative control of DC microgrids is presented in [31]. Reference [32] discusses the application of distributed control for voltage

regulation and current sharing in DC microgrids. There are many strategies within the distributed control approach as discussed in [33]. A multi-agent based distributed control approach is presented in [34] and a consensus-based approach is discussed in [35].

1.4 Communication Requirements in Microgrids

Communication is an essential component in microgrids as it facilitates demand response, power quality improvement, integration of renewable energy sources, privacy and security [36]. Communication in microgrids can be applicable at different levels including primary, secondary and tertiary. For example, a voltage-frequency bus-signaling method is used for coordination of DERs in an islanded microgrid [37]. A low bandwidth communication infrastructure for secondary control and grid synchronization of microgrids is discussed in [38]. Communication is also required for tertiary control where there is an exchange of power between the microgrid and distribution network [39]. Hence designing a suitable communication network is critical for microgrid applications.

1.5 Thesis Outline

The rest of the thesis is organized as follows:

Chapter 2: Communication Background

Chapter 2 describes the different wired and wireless communication techniques used in power systems. The techniques are compared and the advantages and suitability of 5G for power system applications is discussed.

Chapter 3: 5G Enabled Co-simulation Environment for Distributed Control

Chapter 3 discusses the Co-simulation environment developed to analyze the performance of a 5G RAN for distributed control in microgrids. The distibuted control applications are developed in PSCAD and the communication network is designed in python.

Chapter 4: Age-Optimal Scheduling for Distributed Control of Microgrids

Chapter 4 discusses age of information as a metric for scheduling in 5G. The performance of an AoI-aware scheduler in distributed control scenarios is analyzed and compared with standard non-AoI–aware schedulers.

Chapter 5: Conclusions

Chapter 5 discusses the contributions of the thesis and general conclusions. It also enumerates future research directions.

Chapter 2

Communication Background

Power systems can require communication for different purposes [40]. These include management (monitoring and control) of distributed energy resources (DER) and energy storage systems as well as providing real time coordination (required for energy exchange) between them. Communication is also required in phasor measurement units (PMU) that are used for grid monitoring. Load management and distribution network supervision also demands an agile communication network. Communication capabilities are also needed in advanced metering infrastructures and electric vehicles. A good communication service can result in better fault management and might ultimately prevent blackouts. Table 2.1 shows the communication requirements for different power system applications.

Different techniques are available to implement a good communication channel in power systems. They can be broadly classified into wired and wireless communication channels.

2.1 Wired Communication Channel

2.1.1 Power Line Communication (PLC)

This technique uses the conventional power lines for communication [41]. The information between the participating devices (DERs or controllable loads) is exchanged at a high speed data rate of around 2–3 Mbps. Communication between phasor measurement units (PMU)

Table 2.1: Communication requirements in different power system applications [2]

Application	**Typical data size (bytes)**	**Typical sampling rate**	**Latency**	**Reliability (%)**
Home automation (thermostat setting, air conditioning (HVAC)	10–100	once every configurable period (1 min - 15 min)	seconds	>98
On-demand meter reading	100	as required	<15 s	>98
Demand response	100	1 per device per broadcast request	<1 min	>99.5
Distribution automation (Volt/VAR control)	150-250	1 per device per 12 h (24 x 7)	<5 s	>99.5
Distribution automation (fault detection, clearing and restoration)	25	1 per device per event (<5 s within <1.5 min of fault event)	<5 s	>99.5
Wide-area protection (adaptive islanding, load shedding)	4–157	once every 0.1 s	<0.1 s	>99.9
Wide-area control (voltage stability and cascading failure control)	4–157	once every 0.5–5 s	<5 s	>99.9
Wide-area monitoring (power oscillation monitoring and PMU-based state estimation)	>52	once every 0.1 s	<0.1 s	>99.9

and phasor data concentrator (PDC) also typically uses power line communication. Urban areas primarily use PLC technology for monitoring and control applications in microgrids.

Advantages:

1. Infrastructure is widely available.
2. PLC is cost effective since already existing power lines are used for communication.

Disadvantages:

1. There is little to no security as power lines are used for communication.
2. Noise and interference due to the power lines can affect communication. Signal quality can also be affected by the wiring distance between the transmitter and the receiver.

Power line communication technique suffers mainly from signal interference and attenuation depending on the length of transmission. Coupled with security related issues, it is not the best option for microgrid communication.

2.1.2 Optical Fiber Communication

Optical fiber communication is typically used in the transmission level that requires communication over long distances [41]. Optical transmitter (laser or LED) is used to convert the measured signal into an optical signal. The signals are then carried to the receiving end as an optical signal wave. The optical signals at the receiver are then converted to electrical signals using photodiodes. Optical repeaters are sometimes placed at regular intervals to boost and maintain the signal quality.

Advantages:

1. Signal quality is maintained since there is negligible interference.
2. Signal attenuation is low thus providing high reliability.
3. Data rates are high.

Disadvantages:

1. Installation costs and time required for installation is high.
2. Scalability in terms of plug-and-play operation of DERs or controllable loads needing communication channels is not good in optical fibres.

Optic fibres are relatively expensive. Their application in microgrid scenarios suffers from the drawback that they are not highly scalable and each DER addition would require significant changes in the infrastructure.

2.2 Wireless Communication Channel

2.2.1 ZigBee

The ZigBee technology is based on IEEE 802.15.4 standard [42]. It is mainly used for wireless personal area networks (WPAN). It makes uses of different routing technologies including tree based algorithm and AODV (Ad hoc On Demand Distance Vector) algorithm [41].

Advantages:

1. The power usage is minimal and no complex equipment is required for operation.

2. ZigBee is economical and cost of deployment is low.

Disadvantages:

1. ZigBee can cause interference with appliances using WiFi, microwave, or Bluetooth.

2. Memory size is less.

3. It has lower processing capabilities compared to other technologies.

ZigBee is a low power and low range communication option is not very suitable if the geographical network coverage is high. It may not support information packets of large size which may be the case in PMU packets or readings from electric meters.

2.2.2 Cellular/Mobile Network Technology

Different cellular technologies (LTE-A, HSPA, UMTS, EDGE and GPRS) can be used for communication requirements in different power system applications [41]. These cellular technologies coupled with the equipment used for communication constitute different generations of mobile technology (1G–5G). They are advantageous as compared to wired communication technologies since they provide accessibility in remote areas, scalability, and have comparatively lower infrastructure cost.

2.3 5G

5G represents the fifth generation of mobile technology and is proposed with an objective to provide faster data rates, higher security, low communication latency and connection for

a large number of devices. The major difference between 5G and the previous generations of mobile technology is in the electromagnetic frequency spectrum. 5G makes use of higher frequency ranges as compared to the frequency used by current generations of mobile technology. There are two frequency ranges used in 5G. The first spectrum utilizes frequencies below 6 GHz (typically around 3.4–3.8 GHz) and is called the "sub-6" or "low- to mid-band spectrum". "High-band spectrum" represents the other frequency range and is typically between 24–100 GHz.

2.3.1 5G Features

5G provides many unique features compared to the older generations of mobile technology. These are listed below.

Millimeter-Wave

The wavelength of an electromagnetic wave is inversely proportional to its frequency as all electromagnetic waves travel at the speed of light. If the 5G network utilizes the high-band spectrum, the wavelength of the 5G waves will be in the millimeter range. Hence waves in this spectrum are also called the mmWave [42]. mmWaves can transmit information at higher speeds, low latency and high security. Due to the short wavelength, they avoid congestion during information transfer.

Massive Multiple-Input Multiple-Output (MIMO)

The characteristics of the 5G mmWave allow for more antennas to be deployed. This is known as the MIMO technology. 5G networks can have 32–256 antennas as compared to 4G communication networks that usually have around 8 antennas [43]. Using MIMO

can result in higher spectral and energy efficiency [43]. The transmission bandwidth and data throughput is improved through massive MIMO [44]. MIMO also provides benefits in interference management [45].

Light Fidelity (LiFi)

To reduce the congestion on the frequency spectrum available for radio frequency communication and to overcome other drawbacks in radio waves, visual light communication facilitated through 5G is becoming more viable as an alternative communication technique [46]. This optical wireless technology is called LiFi and provides low interference, low power consumption and high spatial reuse.

Ultra-Dense Cellular Networks

Due to the short wavelength of mmWaves, the transmission distances is reduced as well. They can also be obstructed by walls and people. Hence signal repeaters are needed in the form of small 5G cells. This ensures good coverage over the entire 5G network and is called as a ultra-dense cellular network [47]. The density of 5G macro base stations is higher than that of 3G and 4G. 5G is anticipated to require 40–50 base stations per square kilometer as compared to 4–5 base stations per square kilometer used in 3G and 8–10 base stations per square kilometer in 4G [47].

Software Defined Networks (SDN)

Software defined networks involve moving the control plane away from the network hardware to allow external control of data through a ”controller” [48]. Using this feature administrators can make changes and introduce different services to the 5G network. This improves

flexibility and programming in 5G networks.

2.3.2 Comparison With Previous Generation Mobile Networks

5G differs from the previous generation of mobile networks (1G-4G) mainly in terms of data rate (speed), latency and capacity in terms number of devices that can be supported. The latency in 5G is typically around 1 ms, which is around 50 times smaller than the latency in the previous generations of mobile communication technology [49]. 5G also uses a different frequency spectrum as compared to the previous generations. Table 2.2 shows the data rates for different generations of mobile communication technology [50]. As seen from the table, 1G has the lowest data rate. It makes use of analog communication which is typically used for voice calls [50]. 2G has a higher data rate and is mainly used for text messaging [51]. 3G has applications in video calling and multimedia messaging because its data rate is around 14.4 Mbps [52]. 4G has a data rate of around 100 Mbps and can be used to implement internet of things (IoT). IoT is used in smart homes, smart buildings and smart electric power systems [53]. However, 4G still has limitations due to latency and the limited number of devices that can be offered service [52]. This issue is addressed by the features provided under 5G mobile communication technology.

Table 2.2: Data rates for different generations of mobile communication technology

Mobile communication technology generation	**Data rate**
1G	2.4–9.6 Kbps
2G	270 Kbps
3G	14.4 Mbps
4G	100 Mbps
5G	>1 Gbps

2.3.3 5G Application Scenarios

eMBB: Enhanced Mobile Broadband

1. It is used for applications requiring fast data transfer services. This is achieved by providing a large bandwidth [52].
2. Peak transfer speed of 20 Gbps can be achieved and an average speed of 10 Mbps can be achieved in each square meter.
3. Typical applications include 3D video, cloud computing and augmented reality.

uRLLC: Ultra-Reliable and Low-Latency Communications

1. It is used in applications requiring remote control with an objective to minimize the latency between the base station and the terminal devices [52].
2. Average latency achieved is around 1 ms.
3. Typical applications include industry automation and automated driving.

mMTC: Massive Machine Type Communications

1. It is used in applications requiring connections among a large number of devices [52].
2. The number of devices supported by the 5G network is around one million per square kilometer.
3. Typical applications include smart homes, smart buildings, and smart cities.

2.3.4 Applications in Power Systems

5G can have different applications in power systems. 5G technology can play a key role in implementation of demand response schemes [40]. Under a demand response program (DRP), consumers can participate in the grid's operation via load shifting or consumption reduction. Interconnecting energy sources in a power system through a 5G network also provides for better energy forecasting and helps manage energy balance [54]. 5G is also proposed to be a viable option in implementing IoT-enabled smart grids [40]. These IoT enabled systems can seek the best solution to maintain security and economy of the power system during contingencies or sudden changes. Integration of 5G can also provide uncertainty management in power systems by providing real-time monitoring over uncertain renewable energy resources [40]. Finally, 5G can also be useful in protection scenarios. Circuit breakers in fault detection schemes are observed to respond faster in a 5G enabled distributed control network compared to a LTE enabled centralized network [55]. Due to the wide range of applications in power systems that 5G can support and improve, there is a need to develop power system structures that are inter-operable with 5G [56].

Chapter 3

5G Enabled Co-simulation Environment for Distributed Control

There has been a recent focus on investigating the benefits that connectivity can bring in smart grids. The authors in [57] compare the response of a fault management system 4G-LTE and 5G systems. The results indicate that machine-to-machine connectivity abilities of 5G provide significant performance improvement compared with 4G. Reference [58] reviews several applications that 5G can enable in smart grids and analyzes the associated challenges. In [59], a network servicing both eMBB (Enhanced Mobile Broadband) and URLLC (Ultra-Reliable and Low-Latency Communications) applications is considered, and its ability in handling line protection through URLLC is analyzed. The results show that provided the network coverage is above a certain threshold, differential line protection can be supported by the network. However, these research studies consider only a black box view of the 5G network without considering the implications of its various subsystems on the overall performance. This paper tries to address this gap.

This section discusses a co-simulation environment for power system and communication networks and employs this in an example application for distributed control. Distributed control techniques in smart grids involve distributed energy resources (DER) that coordinate for higher reliability and performance [60], especially where centralized control is impractical. This can happen due to a large number of DERs, privacy and security requirements, and

computational implications. Distributed control can be applied at different levels, including primary [61] and secondary [28].

The contributions of this work are

- A Python-based 5G radio access network (RAN) simulator is developed to interface with general purpose power systems simulators such as PSCAD and MATLAB, thereby creating a co-simulation environment where the power grid components can communicate with each other through 5G links. This allows us to simulate the effects of RAN resource allocation on the smart grid. The RAN simulator is robust in terms of both interfacing with the different software environments and the number of devices that communicate within the power system.
- The suitability of 5G in supporting the specific use cases of a power park and coordinated set point modulation is investigated using this co-simulation environment.
- The performance of the smart grid under a 5G network is compared with an ideal scenario where the power grid components can communicate instantaneously.

3.1 Co-simulator Design

The co-simulation environment is developed to investigate microgrid performance in the presence of a 5G RAN. The power system scenarios are simulated in software tools PSCAD and MATLAB, and the communication environment is implemented through a Python script.

The Python script models the 5G communication that the DERs use in the microgrid for implementing distributed control. Consider the scenario shown in Fig. 3.1. The DERs generate packets containing their state information, i.e., their local measurements. This

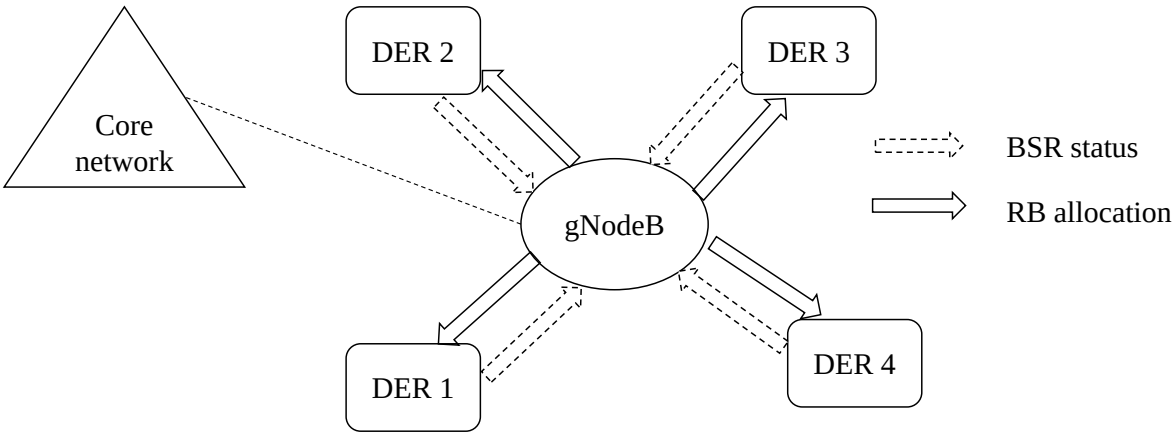

Figure 3.1: Schematic diagram of a 5G Radio Access Network (Core network is not included in RAN as core connectivity is fixed).

information is communicated to other DERs to achieve the distributed control objective. This transmission can be done when the DERs are allocated resources by the 5G Base Station (gNodeB). The resource are means to support the communication links. In 5G, these resources are termed resource blocks (RB). RBs are allocated based on the number of packets a DER wants to transmit. This is known as that DER's buffer status report (BSR).

3.1.1 Co-Simulator Structure

The general design of the co-simulator is shown in Fig. 3.2.

The following algorithm explains the working of the co-simulator in further detail:

1) For the control operation within a microgrid, the DERs might need to communicate with each other. Each DER has information that needs to be sent to other DERs. This information is sent as packets. The number of packets required to be sent for each DER is stored in a text file called the buffer status report (BSR). The channel through which these packets are transmitted among DERs and the scheduling of communication resources for

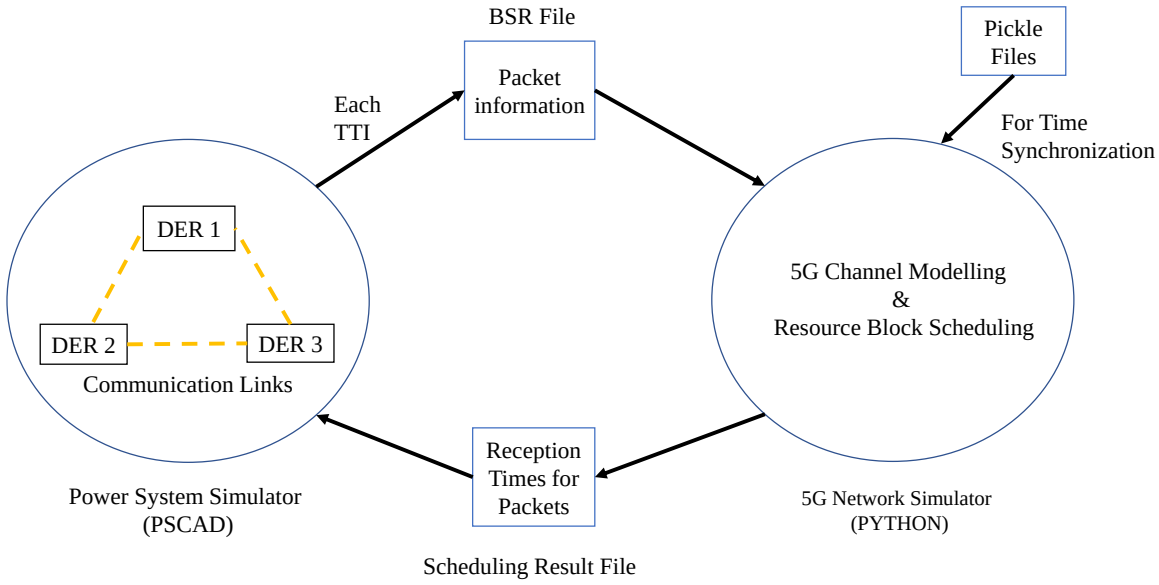

Figure 3.2: Design of the proposed co-simulator (developed in collaboration with Wireless@VT and published in [1]).

this process is simulated with the help of a 5G network simulator created in Python.

2) At each transmission time interval (TTI), this BSR is sent by the power system simulator to the 5G Python simulator. The information to be transmitted is stored internally within the power system simulator.

3) The python simulator representing the 5G communication channel reads this BSR and allocates resource blocks according to availability and channel conditions. It also keeps track of the current simulation time slot and state of the system (information related to previous time slots) with the help of pickle files. If a particular DER is not allocated resource blocks, it would not be able to communicate information to other DERs and this could negatively affect the dynamic performance and set point tracking of other DERs. Hence the scheduler keeps track of this and gives more priority to that particular DER in the next TTI.

4) Based on allocated resource blocks and channel conditions the throughput is calculated. This then decides the reception time for each packet (the time when the destination DER would receive the packet).

5) This information is written into another text file and read by the power system simulator.

6) The information stored internally in the power system simulator is then sent to the destination DERs at the reception times provided by the python simulator.

7) This process is repeated at each TTI.

3.2 Communication System Design

A round-robin policy π is used for scheduling. In round-robin, equal number of RBs are granted to each DER in a circular fashion, i.e., RBs are allocated to each DER in turn. Each DER also transmits channel state information reference signal (CSI-RS) to gNodeB. This is an of channel quality and is called channel quality index (CQI). CQI provides information about the modulation order that can be used, where modulation order is the number of symbols that can be transmitted. Better CQI allows the use of higher modulation order. The channel is modeled as a random time-varying channel. This causes a varying modulation order over the allocated RBs. The throughput achieved will be higher if the modulation order is higher. M RBs are considered and based on the RB allocation, the throughput achieved in Mbps in each of the communication link is calculated as per 3GPP TS 38.306 [62]. This is shown in (3.1).

$$10^{-6} \sum_{j=1}^{J} (v_{\text{Layers}}^{(j)} Q_m^{(j)} f^{(j)} R_{\max} \frac{12 N_{PRB}^{BW(j),\mu}}{T_s^{\mu}} (1 - OH^j)) \tag{3.1}$$

Here J is the number of carriers aggregated in a carrier aggregation scenario. In 5G, up to 16 carriers can be aggregated. v^j_{Layers} is the maximum number of layers in the jth component carriers (CC). It is also the number of streams and is restricted by the number of antennas used. $Q^{(j)}_m$ defines the modulation order used which depends on CQI. $f^{(j)}$ is the scaling factor used to scale throughput for various CC combinations. $R_{\max}$ is the maximum coding rate and is typically set to $\frac{948}{1024}$ [63]. $N^{BW(j),\mu}_{\text{PRB}}$ is the number of RBs allocated to a single DER. μ defines the 5G numerology selected, and this numerology decides the symbol time, T^{μ}_s, calculated as $T^{\mu}_s = \frac{10^{-3}}{14.2^{\mu}}$. Finally, the overhead $OH(j)$ for carrier j is decided by the frequency band used (FR1 or FR2). gNodeB and DERs communicate in the the FR1 band [64] (410 MHz to 7.125 GHz) using a bandwidth of B. Bandwidth is the range of radio wave frequencies allocated from the FR1 band. This achieved throughput decides the instants of information receptions at the DERs.

The communication parameters used in the simulation are shown in Table 3.1. Aggregated carriers refers to the technique of combining communication resources that increases data rate. Modulation order determines how many bits of information can be carried by a single resource block [65]. Bandwidth refers to the maximum amount of data that can be transmitted in a particular time [66]. Throughput then refers to the amount of information that is actually delivered after considering latency, channel speed, packet loss and other factors. The definition of 5G numerology according to 3GPP specifications is 'sub-carrier spacing type' [67]. In time domain, communication resources are allocated in intervals (TTI) of 1 millisecond. However, some applications might need a much lower latency. An increase in numerology (range: 0–4) would result in increase in the sub-carrier spacing which ultimately results in a TTI lower than the standard 1 millisecond.

The BSR and CQI reports are assumed to be sent out of band (without the need of resources for transmission) and are assured error-free reception at the gNodeB [68]. Therefore the

gNodeB always knows the BSR and CQI at each TTI. The 5G RAN is connected to a core network (CN). As CN is a fiber cable-based network, the delay and reliability of this RAN-CN connection is fixed and do not vary [59]. Therefore, we do not model the CN and instead focus on the RB allocation in the RAN network. As a result, the network performance is investigated from the perspective of RB allocation.

Table 3.1: Parameters used to set up the simulation (developed in collaboration with Wireless@VT and published in [1])

Parameter	**Value**
Aggregated carriers J	2
Modulation order $Q_m^{(j)}$	2, 4, 6, 8
Maximum layers for jth carrier $v_{\text{Layers}}^{(j)}$	2
Scaling factor $f^{(j)}$	0.8
Numerology μ	2
Number of RBs M	3
RBs allocated per DER $N_{\text{PRB}}^{\text{BW(j)}}$	1
Scheduling policy π	Round robin
BSR periodicity τ	1 ms
Transmission time interval TTI	1 ms
Carrier frequency f_D	2.63 GHz
Bandwidth B	5 MHz
Packet size L	150 Bytes [69]

3.3 Use Case I: Power Park

3.3.1 System Description

This case involves distributed control of N inverters connected to a common bus [61], as shown in Fig. 3.3.

This case employs frequency partitioning, which divides the control tasks between the remote central controller and the distributed local controllers of each inverter. The concept of

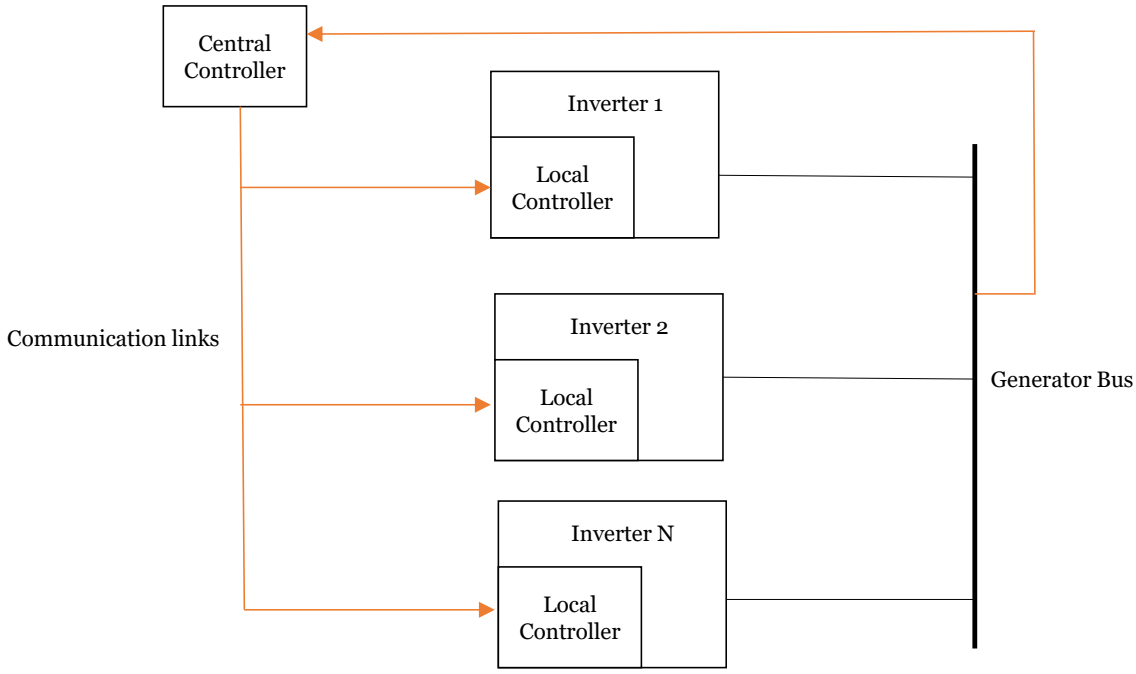

Figure 3.3: Power park system model.

frequency partitioning is shown in Fig. 3.4. This method reduces the required communication bandwidth between the remote central controller and the local controllers. The low frequency component of the control signal is provided by the central controller, while its high frequency component is generated by the local controllers. $y^{\star}$ denotes the reference signal for the central controller. The reference signal for the local controller is set to zero because disturbance rejection is desired at high frequency. LPF, and HPF represents the low pass and high pass filters.

The test system under consideration has three inverters, where each inverter contains an inner current control loop embedded within an outer voltage control loop. A 5G network is used to communicate the control signals from the central controller to the individual local controllers at each inverter. The inverters and loads are connected to the generator bus. Further details about this case can be found in [61].

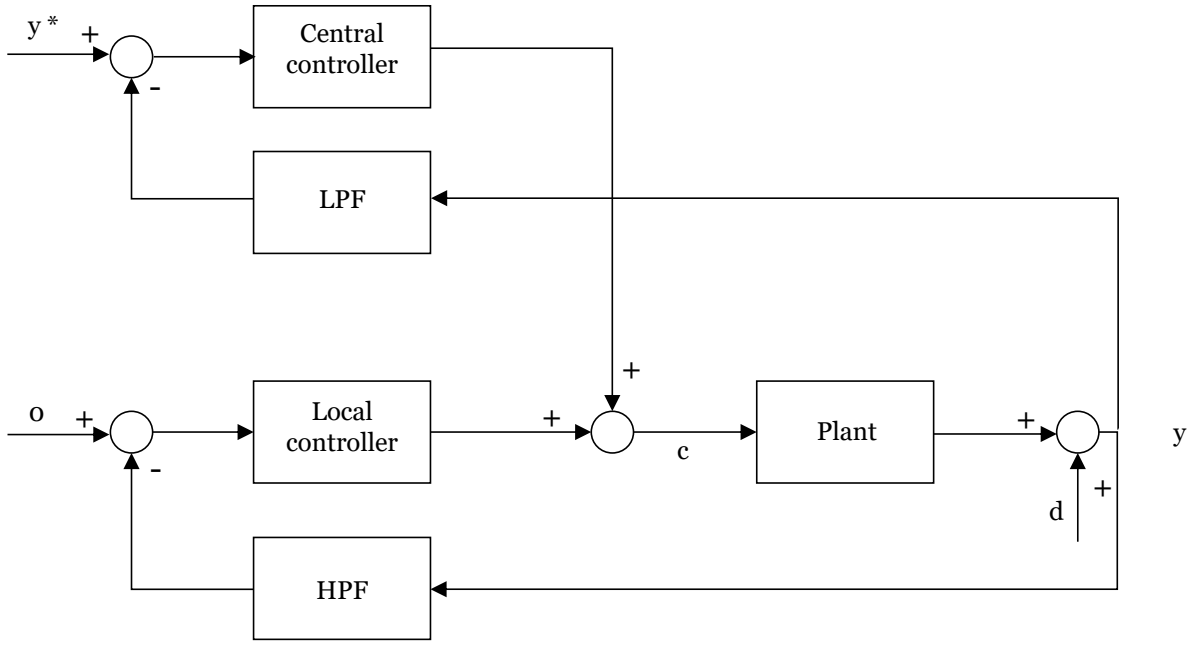

Figure 3.4: Frequency partitioning for inverter control.

3.3.2 Performance Evaluation

Set Point Change in Voltage at the Generator Bus

This case study evaluates voltage regulation at the common generator bus. The analysis is carried out in the *dq*-frame of reference. V_{oq} is set to zero and a step change is applied in V_{od} from 0.2 to 0.3 at $t = 0.07$ s. The system response is shown in Fig. 3.5. $V_{\text{od-ideal}}$ denotes the system simulation response under ideal conditions (5G channel is not used). $V_{\text{od-5G}}$ denotes the system response with 5G communication channel (the low frequency control signal is communicated from the central controller to the individual local controllers). Table 3.2 shows the overshoot and settling time of the responses. The settling times for both the cases are around 0.01 s. There is, however, a change in overshoot from 1% to 10.3% in the presence of the 5G network.

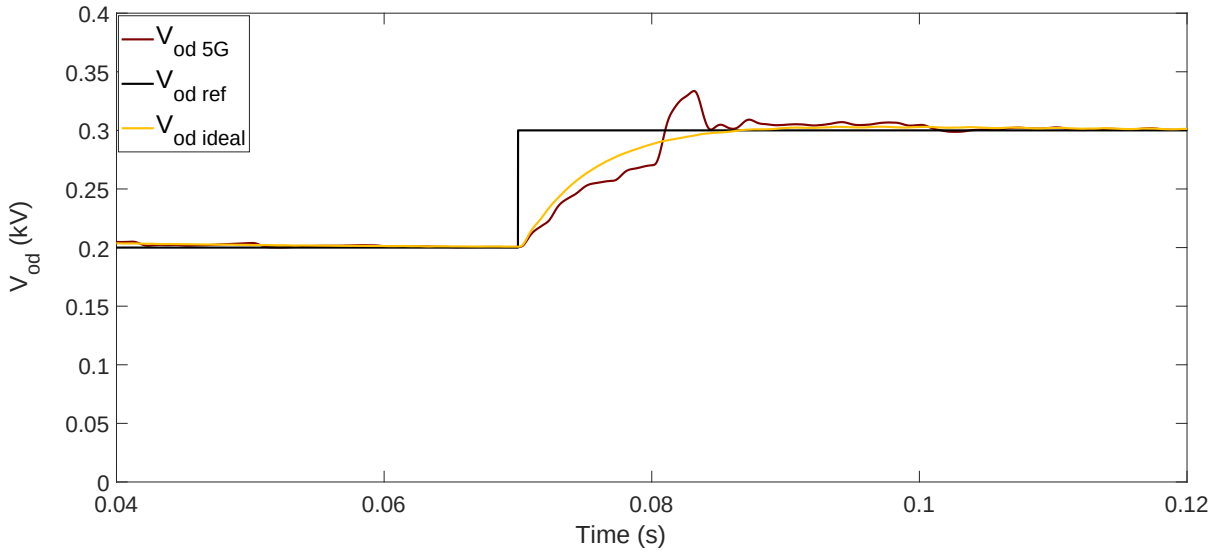

Figure 3.5: Comparison of the system response (d-component of the voltage at the generator bus) to a step change in set-point with and without the 5G network.

Table 3.2: Overshoot and Settling time for set point change in voltage at the generator bus (Power park case)

Case	Overshoot (%)	Settling Time (ms)
Ideal	1	11.1
5G	10.3	14.19

Load Switching

The system with and without 5G communication network is subjected to a load switching condition. A three-phase balanced RL load is switched on and is connected to the system at $t = 0.08$ s. The transient response is shown in Fig. 3.6. This includes the d-axis component of the output voltage in dq-frame of reference. The results indicate similar transient performance for both cases. The transient lasts for around 5 ms in both the cases and the system does not lose its stability. The drop in voltage is around 0.01 V more with the 5G channel.

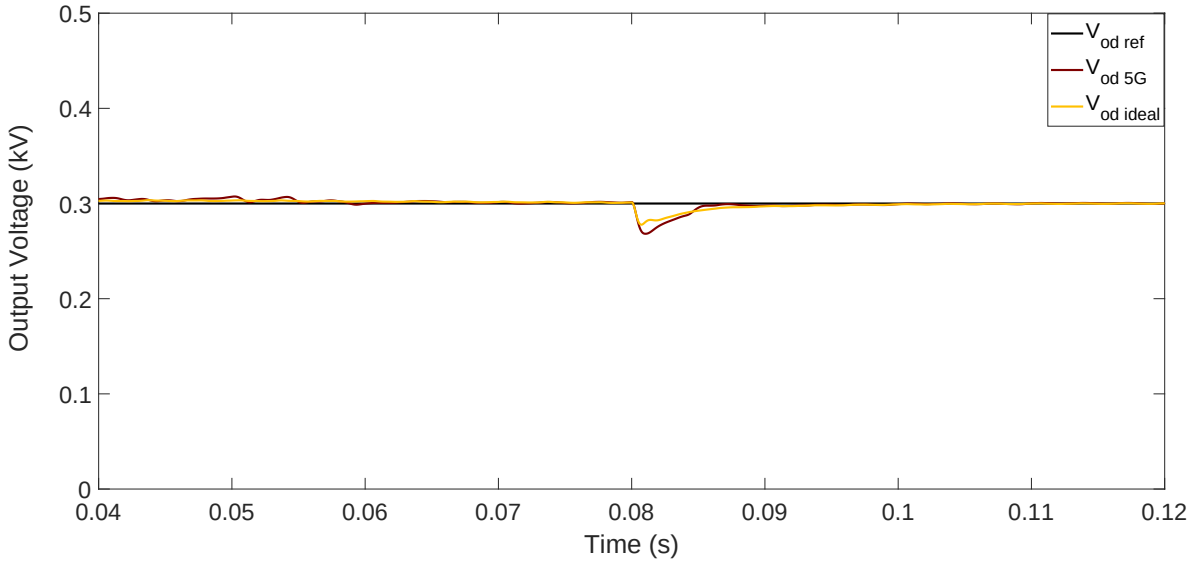

Figure 3.6: Load switching of a three phase balanced RL load. Output voltage in dq frame (d-axis component).

Single-Phase to Ground Fault at the Generator Bus

A single-phase A-G fault is simulated at $t = 0.08$ s for 0.03 s at the generator bus. Fig. 3.7 shows the results. The system with 5G network does not lose its stability. It is able to continue tracking the reference value of the direct axis voltage at the generator bus after the fault is cleared. The transient lasts for about 0.065 s after the fault is cleared with 5G channel, while it lasts for around 0.028 s with ideal communication.

Three-Phase to Ground Fault at the Generator Bus

A three-phase ABC-G fault is simulated at $t = 0.08$ s for 0.03 s at the generator bus. Fig. 3.8 shows the results. The system with 5G network does not lose its stability. It is able to continue tracking the reference value of the direct axis voltage at the generator bus after the three-phase to ground fault is cleared. The transient lasts for 0.13 s after the fault is

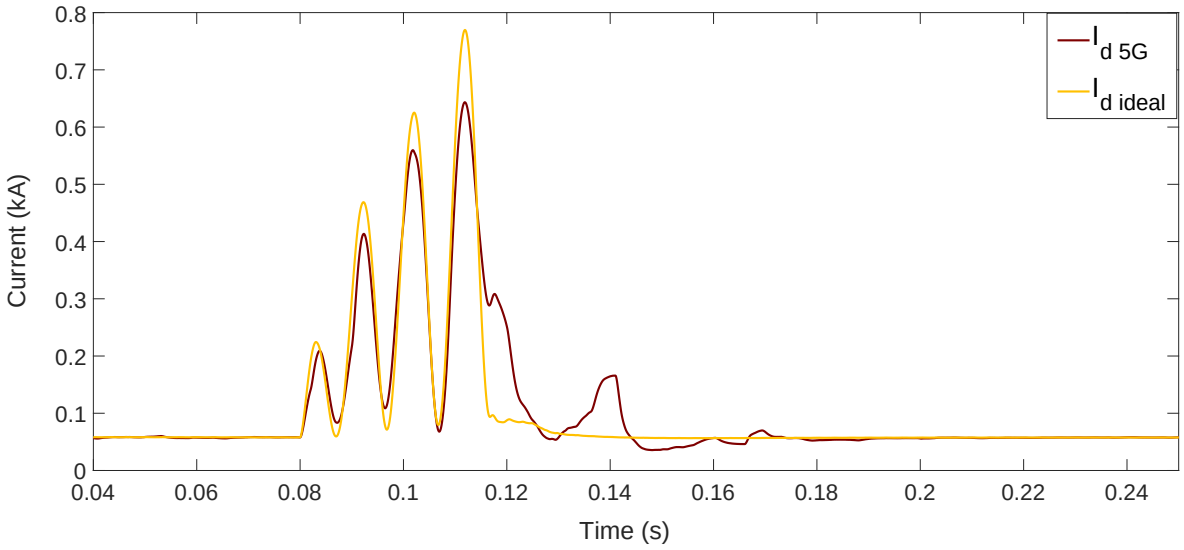

(a)

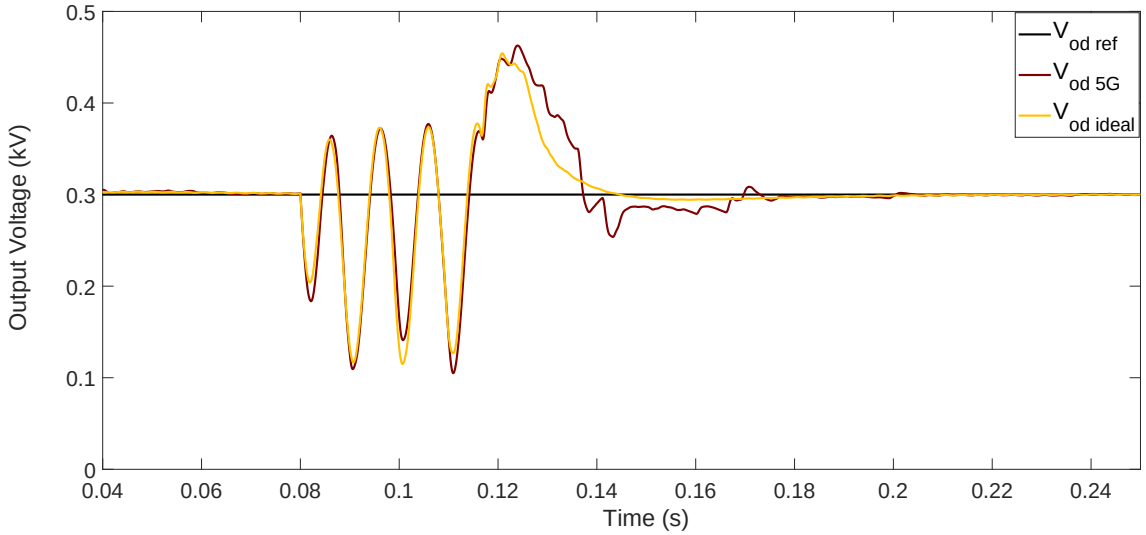

(b) s

Figure 3.7: Single-phase fault to ground (a) *d*-component of the output current of one of the inverters in *dq*-frame. (b) *d*-component of the output voltage at the generator bus in *dq*-frame.

cleared with 5G channel, while it lasts for 0.1 s with ideal communication.

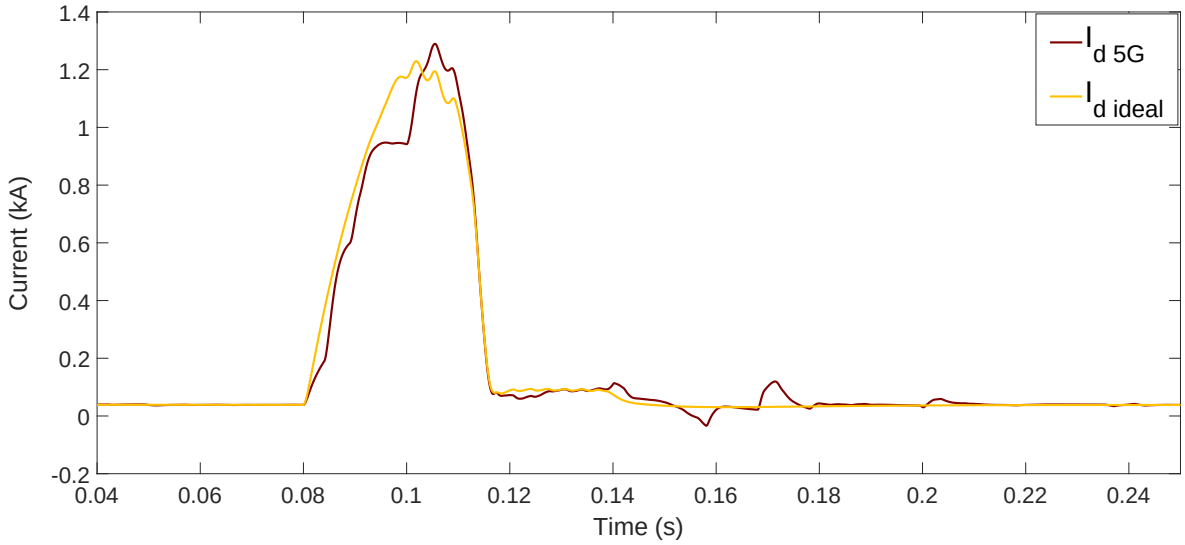

(a)

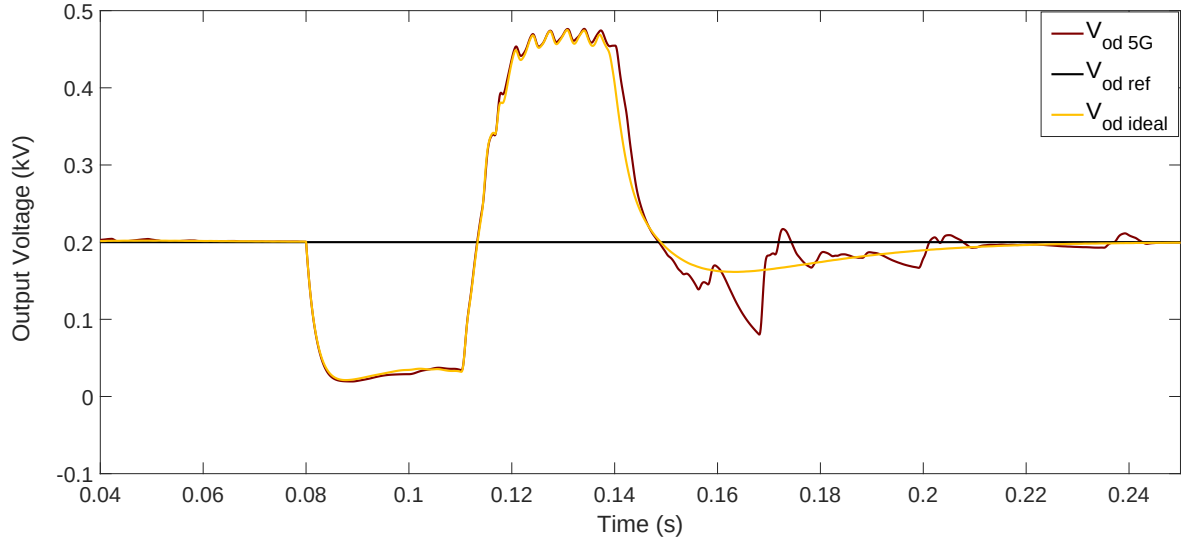

(b)

Figure 3.8: Three-phase fault to ground (a) *d*-component of the output current of one of the inverters in *dq*-frame. (b) *d*-component of the output voltage at the generator bus in *dq*-frame.

3.4 Use Case II: Coordinated Set Point Modulation of DERs

3.4.1 System Description

The dynamic response of DERs in a microgrid can be improved using a method called as set point modulation [70]. The objective of this method is to get a response that has shorter settling time and smaller overshoot. This is achieved by adjusting the set point of a DER y_{sp} between original and scaled values to achieve better tracking performance $y(t)$. These scaled values are evaluated based on the instantaneous response of the DER and its overall trend. Set point can refer to any electrical quantity that is being controlled, e.g., voltage, current, or power. Modulation in this context, refers to adjusting the set point based on the trend of DER response and its sampled values. Mathematically, set point modulation can be expressed as

$$y'_{\text{sp}} = y_{\text{sp}} + me(t). \tag{3.2}$$

Here y'_{sp} represents the modulated set point, m is a design parameter, and $e(t)$ is the tracking error which is given by

$$e(t) = y_{\text{sp}} - y(t). \tag{3.3}$$

To further reduce settling time and overshoot, the predictive dynamic behavior of the tracking error can be used. That is,

$$y'_{\text{sp}} = y_{\text{sp}} + m\hat{e}_{\text{pred}}(t). \tag{3.4}$$

In this work, a linear predictor is used to obtain $\hat{e}_{\text{pred}}(t)$ as it is more suitable for real-time implementation due to reduced computational requirements and simple implementation.

The above equations represent a single DER. To achieve fast and improved dynamic response in a scenario where multiple DERs operate, coordination between DERs is needed. This is achieved through coordinated set point modulation [28]. Consider N DERs participating in coordinated set point modulation that are capable of exchanging information over a communication channel. The predicted tracking errors of each DER $\hat{e}_{\text{pred}}(t)$ are shared with the other DERs that are connected through a communication link. The modulated set point of the ith DER is given as

$$y'_{i_{\text{sp}}} = y_{i_{\text{sp}}} + m_i \hat{e}_{i_{\text{pred}}}(t). \tag{3.5}$$

The above set point equation can be modified to include the coordinated set point modulation of N DERs. The term representing this coordination $v(t)$ is defined as

$$v(t) = m_i \sum_{j=1, j\neq i}^{N} a_{\text{ij}} \hat{e}_{j_{\text{pred}}}(t), \tag{3.6}$$

where a_{ij} denotes a communication link between DER i and DER j. The control equation can then be represented by

$$y_{i_{\text{sp}}} = y_{i_{\text{sp}}} + m_i \hat{e}_{i_{\text{pred}}}(t) + m_i \sum_{j=1, j\neq i}^{N} a_{\text{ij}} \hat{e}_{j_{\text{pred}}}(t). \tag{3.7}$$

Further details about this concept can be found in [28].

3.4.2 Performance Evaluation

Fig. 3.9 shows the three devices (DERs) that interact with each other using coordinated set-point modulation.

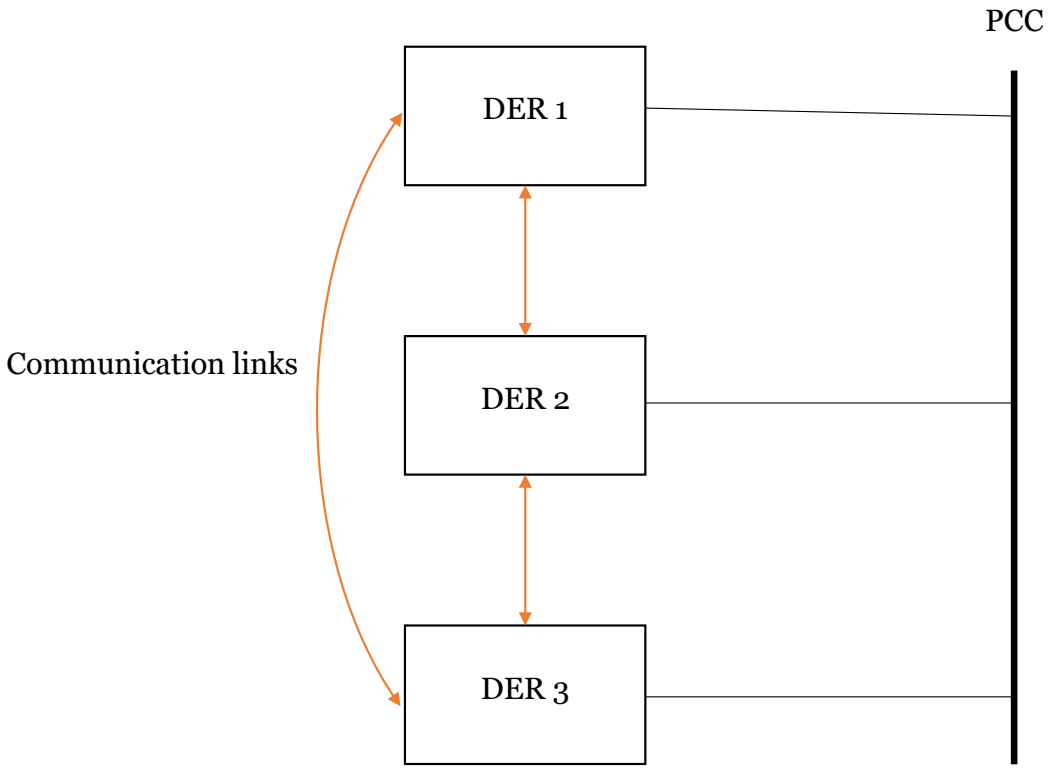

Figure 3.9: System model of coordinated set point modulation of DERs.

Staggered Set Point Change

A staggered set point change is applied to the individual devices (step change in reference point from 0 to 1 at $t = 0.5$ s for DER 1, at $t = 1$ s for DER 2 and at $t = 1.5$ s for DER 3). These set points can represent any electrical quantity that needs control (voltage, real power or reactive power). The combined system response at the PCC, under ideal simulation

conditions (no 5G communication involved) and in the presence of a 5G network, is shown in Fig. 3.10. Table 3.3 shows the overshoot and the settling time of the system response under the two conditions. The settling time increases by 172 ms in the presence of a 5G network and the overshoot is twice the ideal simulation condition. However, the DERs are able to track the set point changes successfully with 5G communication.

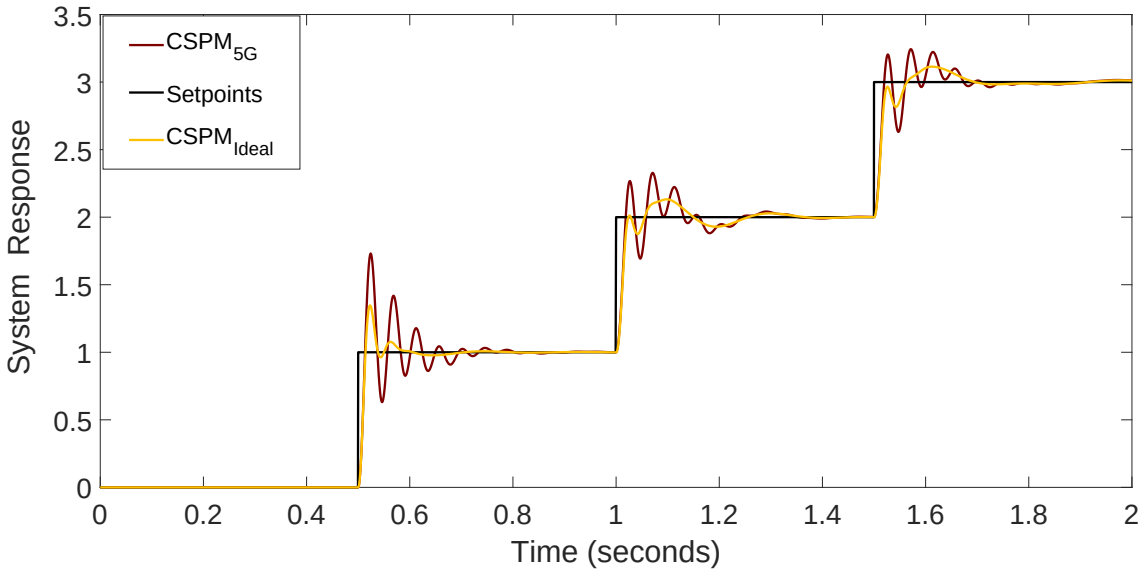

Figure 3.10: Comparison of system response for coordinated set point modulation (staggered set point change) with and without 5G network.

Simultaneous Set Point Change

A simultaneous set point change is applied to all the devices (step change in reference point from 0 to 1 at $t = 0.5$ s). The set point is brought back to 0 for all the devices at $t = 2$ s. The combined system response at the PCC, under ideal simulation conditions and in the presence of a 5G network, is shown in Fig. 3.11. Table 3.3 shows the overshoot and the settling time of the system response under the two conditions. The settling time increases by 84 ms in the presence of a 5G network and the overshoot is higher by 11.4%. However,

the set points are tracked successfully without loss in stability.

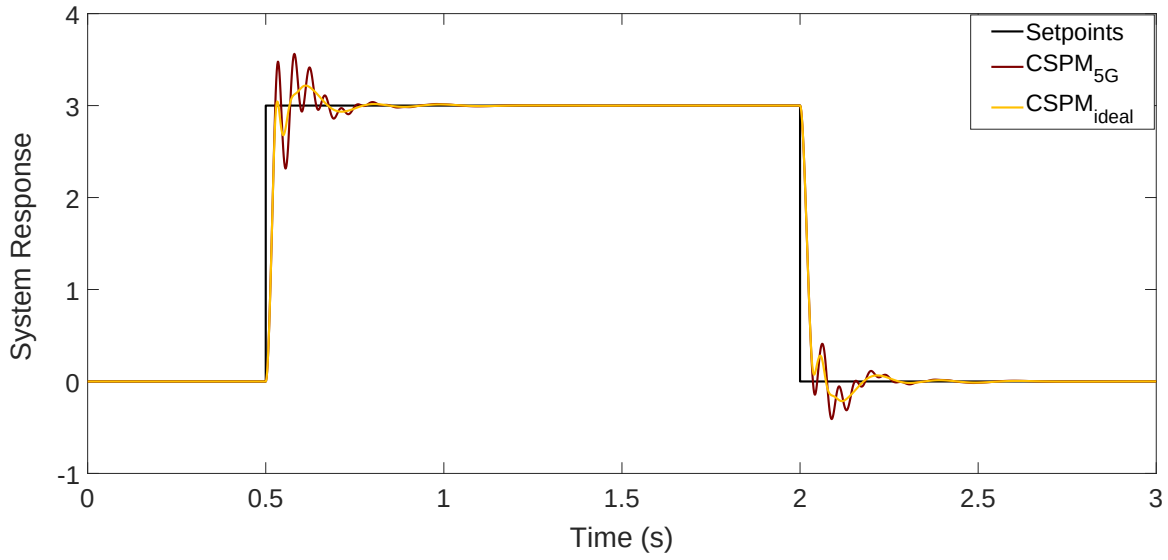

Figure 3.11: Comparison of system response for coordinated set point modulation (simultaneous set point change) with and without the 5G network.

Communication Failure in One of the Devices

The system performance is evaluated when one of the devices is incapable of communicating its state to the other two devices. The response is shown in Fig. 3.12. The response is also compared with the scenario in which all the devices can communicate without any hindrance. Although there is an increase in overshoot and settling time, the system is able to track the set points owing to the control algorithm used. This can be seen from the first two terms in (3.7). These terms do not depend on the states of the other devices, thus contributing towards set point tracking in the absence of information from one device.

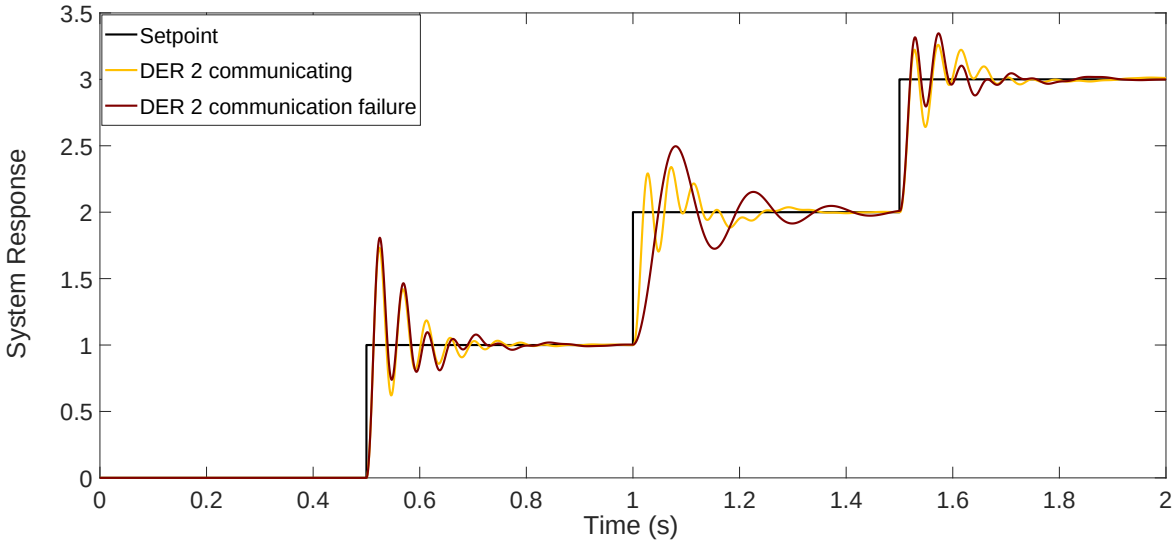

Figure 3.12: Comparison of system response for coordinated set point modulation (staggered set point change) under ideal communication conditions and when communication for device 2 fails.

Table 3.3: System Performance for set point changes (Coordinated set point modulation case)

Set point change	**Case**	**Overshoot (%)**	**Settling Time (ms)**
Staggered	Ideal	34	78
	5G	73.1	250
Simultaneous	Ideal	7.2	153
	5G	18.6	237

Chapter 4

Age-Optimal Scheduling for Distributed Control of Microgrids

Most of the works investigating communications in power systems use delay, throughput, and other traditional metrics to analyze the communication network [71, 72, 73]. However, such metrics fail to capture the timeliness and freshness of the information being communicated. To account for the freshness of information, a new metric called age of information (AoI) has been recently proposed and investigated for a variety of time-sensitive systems including vehicular networks and UAV-assisted IoT networks. In [74] and [75], the authors show that minimizing AoI is an important factor in improving the safety of vehicular networks. In [76], transmission parameters like code-word length, encoding, and retransmissions are optimized for vehicular networks in a space-air-ground integrated network. Similarly, the authors in [77] use deep learning to design driving routes for vehicle to improve AoI. Improving AoI in UAV-assisted IoT networks has been investigated in terms of scheduling in [78, 79] and trajectory selection in [80, 81, 82]. However, AoI has not been explored in the context of microgrids. Microgrids are an essential application for 5G and it is important that AoI performance in it is investigated.

This section focuses on the scheduling aspect of a 5G radio access network (RAN). The AoI performance of four different schedulers, i.e., maximal age difference (MAD), maximal age first (MAF), proportional fairness (PF), and round robin (RR), are investigated. Then

using a co-simulation platform where the DERs communicate under a 5G base station for distributed control, the impact of the schedulers on the microgrid performance is analyzed. Two test systems employing distributed control are considered: IEEE 34-bus system and the CIGRE distribution system. The IEEE 34-bus system works in grid-connected mode while the CIGRE system works in the islanded mode. The number of DERs communicating in the CIGRE system (28) is considerably higher than the IEEE 34-bus distribution system (3). The results show that the microgrid has better set point tracking under schedulers that minimize AoI. The contributions of this work are

- A co-simulation environment is developed to model a 5G RAN facilitating scheduling among DERs in different microgrid test cases.
- Performance of different 5G schedulers is compared in terms of the average AoI achieved for grid-connected and islanded modes of operation of the microgrid.
- The performance of different schedulers is investigated with varying number of DERs.

4.1 Communication Network Description

A wireless coverage is provided to the microgrid through a 5G network [3]. This enables communication among the DERs. An adjacency matrix A represents the communication links between the DERs. Here $a_{\text{ij}} = 1$ means DER i sends packets containing its local measurements to DER j, and $a_{\text{ij}} = 0$ means that DERs i and j do not communicate. The packet generated at DER i is first uploaded to the 5G base station (BS). This is then transmitted from the BS to DER j in the downloading step. Table 4.1 shows an example of the adjacency matrix. Source DERs (denoted by G) generate packets to be uploaded to

the BS. The DERs receiving these packets are the destination DERs and denoted as R. A particular DER may be in both R and G.

4.1.1 5G Communication Network Model

In the netork model used in this work, the uplink and downlink happen independently at the same time over different frequencies. This is known as the frequency division duplex (FDD) configuration. In FDD, the allocated frequency is split into two parts. This first part is used in uplink to upload packets and the second link is used in downlink to download packets. The BS decides which DERs are allowed to upload and download packets. The uplinks upload packets generated at the G DERs to the BS. Downlinks download these packets from the BS to the R DERs.

Time domain is equally slotted into transmission time intervals (TTI) under 5G. Correspondingly, in the frequency domain, bandwidth (the range of radio wave frequencies that are allocated), is equally partitioned into orthogonal subcarriers. These subcarriers are responsible for carrying the packets. At each TTI, the transmission is scheduled. A group of 12 subcarriers over a TTI make a resource block (RB). The BS keeps two RB pools. One corresponds to the uplink and the other corresponds to the downlink [83]. These RBs have to be allocated to the DERs at each TTI using the following criteria:

- B_u represent the RBs used for uploading packets from DERs in G to the BS. $|G|$ is the maximum number of possible uplinks. Here $||$ denotes cardinality. Therefore, the scheduler has to assign B_u RBs among the $|G|$ possible uplinks.
- B_d represent the RBs used for downloading packets from the BS to the DERs in R. A particular DER $i \in R$ may be receiving packets from $\bar{i}$ other DERs where $\bar{i} \geq 1$. For example, a DER may need voltage measurements from two other DERs as input.

Hence the set of all downlink channels from the BS is given by $\bar{R}$ where $|\bar{R}| = \sum_{i=1}^{R} \bar{i}$ and $|\bar{R}| \geq |R|$. The scheduler needs to assign B_d RBs to the $|\bar{R}|$ possible downlinks.

In the example shown in Table 4.1, $N = 3$, $G = 3$, $R = 2$, $\bar{R} = 4$. All the three DERs upload their packets to the BS. Then the packets from DER 1 are downloaded by DER 2, packets from DER 2 are downloaded by DER 1, and packets from DER 3 are downloaded by DERs 1 and 2.

Table 4.1: An example adjacency matrix representing communication links between DERs

	DER 1	DER 2	DER 3
DER 1	0	1	0
DER 2	1	0	0
DER 3	1	1	0

The channel conditions, traffic model and RB allocation process used in the 5G communication network have been described in detail in [3].

4.1.2 Age of Information (AoI)

Information freshness is quantified using AoI. It is defined and measured as the time elapsed since the generation of the most recently received packet. This is equal to the delay at instants of packet reception and increases linearly during the inter-arrival time. The delay is calculated as the difference between the packet's reception time and generation time. At TTI τ, the AoI corresponding to DER i at the BS is denoted by $\text{AoI}_i(\tau)$, and AoI of DER i at DER j is denoted as $\text{AoI}_{i,j}(\tau)$, where $i \in G$ and $j \in R$. AoI_i is calculated as

$$\text{AoI}_i(\tau) = \tau - g_{u,i}, \tag{4.1}$$

where τ is the ongoing TTI, and $g_{u,i}$ is the generation time of the most recently uploaded packet of DER i that is received successfully at the BS. Similarly, $\text{AoI}_{i,j}(\tau)$ is calculated as

$$\text{AoI}_{i,j}(\tau) = \tau - g_{d,i}, \tag{4.2}$$

where τ is the ongoing TTI, and $g_{d,i}$ is the generation time of the most recently downloaded packet of DER i that is received successfully at DER j. If the DERs do not communicate, i.e., $a_{i,j} = 0$ as per the adjacency matrix, $\text{AoI}_{i,j}(\tau) = 0$. The time average AoI of the source DERs G at the BS is

$$\text{AoI}^{\text{BS}}(T) = \frac{1}{T}\sum_{\tau=1}^{T}\sum_{i=1}^{|G|}\text{AoI}_i^{BS}(\tau). \tag{4.3}$$

Information freshness is measured as the time averaged AoI of all the source DERs at the destination DERs:

$$\text{AoI}(T) = \frac{1}{T}\sum_{\tau=1}^{T}\sum_{i=1,j=1}^{i=|G|,j=|R|}\text{AoI}_{i,j}(\tau) = \frac{1}{T}\sum_{\tau=1}^{T}\sum_{k=1}^{|\bar{R}|}\text{AoI}_k(\tau). \tag{4.4}$$

To improve the information freshness at the destination DERs, $\text{AoI}(T)$ is minimized with the constraint of the number of available RBs:

$$\begin{aligned} &\min \text{AoI}(T) \\ &\text{such that} \sum_{i\in G} B_i^{\text{alloc}}(\tau) \le B_u, \quad \tau = 1, 2, \ldots, T \\ &\qquad \sum_{i\in G, j\in R} B_{i,j}^{\text{alloc}}(\tau) \le B_d, \quad \tau = 1, 2, \ldots, T \end{aligned} \tag{4.5}$$

where the constraints restrict the number of RB allocations to the total RBs available. At each TTI τ, the scheduler has to choose the following:

- Number of RBs allocated to each DER in the UL. This is represented as $B_U^{\text{alloc}}(\tau) = \cup\, B_i^{\text{alloc}}(\tau)\ \forall i \in G$.
- Number of RBs allocated to each DER in the DL. This is represented as $B_D^{\text{alloc}}(\tau) = \cup\, B_{i,j}^{\text{alloc}}(\tau)\ \forall i \in G$ and $j \in R$.

4.2 Studied Schedulers

In this section, four different schedulers are evaluated on the basis of their AoI and microgrid performance. The schedulers are divided into two broad classes: AoI-based schedulers and non-AoI-based schedulers.

4.2.1 AoI-Based Schedulers

Maximal Age Difference (MAD) Scheduler

The MAD scheduler focuses on the DERs with highest AoI at the BS for uploading, and the highest AoI difference between the BS and destination for downloading [3]. The MAD scheduler is shown in Algorithm 1. The inputs to the algorithm are the current AoI at the BS and destinations for all the DERs. For the uploading step, the DERs are ordered based on their AoI at the BS in line 3. Based on the ordering, the RBs from the B_u pool are allocated in lines 4–7. Similarly for the downlink, lines 8–12 describe how RBs are allocated from the B_d pool to the DERs with the highest AoI difference. This AoI difference is calculated as

$$\text{AoI}_{i,j}^{\text{diff}}(\tau) = \text{AoI}_{i,j}(\tau) - \text{AoI}_i^{\text{BS}}(\tau). \tag{4.6}$$

Algorithm 1 MAD scheduling at TTI τ (developed in collaboration with Wireless@VT and submitted in [3])

Input: $\text{AoI}_i(\tau)$ and $\text{AoI}_{i,j}(\tau)\ \forall\ i \in G$ and $j \in R, B_u, B_d,\ B_i^{\text{need}}(\tau)\ \forall\ i \in G,\ B_{i,j}^{\text{need}}(\tau)\ \forall\ i \in G$ and $j \in R$.
Output: $B_U^{\text{alloc}}(\tau), B_D^{\text{alloc}}(\tau)$.

1: $B_u^{\text{avail}}(\tau) = B_u, B_d^{\text{avail}}(\tau) = B_d$
2: **for** $l = 1, 2, ..$ **do**
3: **for** $i \in G$ with lth highest $\text{AoI}_i(\tau)$ **do**
4: **if** $B_u^{\text{avail}}(\tau) > 0$ **then**
5: $B_i^{\text{alloc}}(\tau) = \min(B_u^{\text{avail}}(\tau), B_i^{\text{need}}(\tau))$
6: $B_u^{\text{avail}}(\tau) = B_u^{\text{avail}}(\tau) - B_i^{\text{alloc}}(\tau)$
7: $B_U^{\text{alloc}}(\tau) = B_U^{\text{alloc}}(\tau) \cup B_i^{\text{alloc}}(\tau)$
8: **for** (i, j) $i \in G$, $j \in R$ with lth highest $\text{AoI}_{i,j}^{\text{diff}}(\tau)$ **do**
9: **if** $B_d^{\text{avail}}(\tau) > 0$ **then**
10: $B_{i,j}^{\text{alloc}}(\tau) = \min(B_u^{\text{avail}}(\tau), B_i^{\text{need}}(\tau))$
11: $B_d^{\text{avail}}(\tau) = B_d^{\text{avail}}(\tau) - B_{i,j}^{\text{alloc}}(\tau)$
12: $B_D^{\text{alloc}}(\tau) = B_D^{\text{alloc}}(\tau) \cup B_{i,j}^{\text{alloc}}(\tau)$

Maximum Age First (MAF) Scheduler

Under MAF, the devices with the highest AoI at both the BS and the destinations are prioritized [3]. See Algorithm 2. The inputs to the algorithm are the current AoI at the BS and destinations for all the DERs. For the uploading step, the DERs are ordered based on their AoI at the BS in line 3. Based on the ordering, the RBs from the B_u pool are allocated as shown in lines 4–7. Similarly for the downlink, lines 8–12 describe how RBs are allocated from the B_d pool to the DERs with the highest AoI at the destination.

4.2.2 Non-AoI–Based Schedulers

Under non-AoI based schedulers, traditional schedulers typically used for 5G are considered.

Algorithm 2 MAF scheduling at TTI τ (developed in collaboration with Wireless@VT and submitted in [3])

Input: $\text{AoI}_i(\tau)$ and $\text{AoI}_{i,j}(\tau)\ \forall\ i \in G$ and $j \in R, B_u, B_d,\ B_i^{\text{need}}(\tau)\ \forall\ i \in G,\ B_{i,j}^{\text{need}}(\tau)\ \forall\ i \in G$ and $j \in R$.
Output: $B_U^{\text{alloc}}(\tau), B_D^{\text{alloc}}(\tau)$.

$B_u^{\text{avail}}(\tau) = B_u, B_d^{\text{avail}}(\tau) = B_d$
for $l = 1, 2, ..$ **do**
  for $i \in G$ with lth highest $\text{AoI}_i(\tau)$ **do**
    if $B_u^{\text{avail}}(\tau) > 0$ **then**
      $B_i^{\text{alloc}}(\tau) = \min(B_u^{\text{avail}}(\tau), B_i^{\text{need}}(\tau))$
      $B_u^{\text{avail}}(\tau) = B_u^{\text{avail}}(\tau) - B_i^{\text{alloc}}(\tau)$
      $B_U^{\text{alloc}}(\tau) = B_U^{\text{alloc}}(\tau) \cup B_i^{\text{alloc}}(\tau)$
  for (i, j) $i \in G$, $j \in R$ with lth highest $\text{AoI}_{i,j}(\tau)$ **do**
    if $B_d^{\text{avail}}(\tau) > 0$ **then**
      $B_{i,j}^{\text{alloc}}(\tau) = \min(B_u^{\text{avail}}(\tau), B_i^{\text{need}}(\tau))$
      $B_d^{\text{avail}}(\tau) = B_d^{\text{avail}}(\tau) - B_{i,j}^{\text{alloc}}(\tau)$
      $B_D^{\text{alloc}}(\tau) = B_D^{\text{alloc}}(\tau) \cup B_{i,j}^{\text{alloc}}(\tau)$

Proportional Fairness (PF) Scheduler

The PF algorithm is designed to take advantage of multi-user diversity, along with maintaining comparable long-term throughput for all users [84]. This is useful in wireless networks that are characterized by time-varying channel conditions. This is explained in Algorithm 3. Once the RBs have been allocated, the average throughput is updated as per equations in [3].

Round Robin (RR) Scheduler

Under RR, the available RBs are assigned in equal and circular fashion among the DERs [85]. While allocating RBs, the channel condition is not taken into consideration.

Algorithm 3 PF scheduling at TTI τ (developed in collaboration with Wireless@VT and submitted in [3])

Input: $R_i(\tau)$, $T_i(\tau), R_{i,j}(\tau)$ and $T_{i,j}(\tau)$ $\forall$ $i \in G$ and $j \in R, B_u, B_d$, $B_i^{\text{need}}(\tau)$ $\forall$ $i \in G$, $B_{i,j}^{\text{need}}(\tau)$ $\forall$ $i \in G$ and $j \in R$.
Output: $B_U^{\text{alloc}}(\tau), B_D^{\text{alloc}}(\tau)$.

$B_u^{\text{avail}}(\tau) = B_u, B_d^{\text{avail}}(\tau) = B_d$
for $l = 1, 2, ..$ **do**
  for $i \in G$ with lth highest $R_i(\tau)/T_i(\tau)$ **do**
    if $B_u^{\text{avail}}(\tau) > 0$ **then**
      $B_i^{\text{alloc}}(\tau) = \min(B_u^{\text{avail}}(\tau), B_i^{\text{need}}(\tau))$
      $B_u^{\text{avail}}(\tau) = B_u^{\text{avail}}(\tau) - B_i^{\text{alloc}}(\tau)$
      $B_U^{\text{alloc}}(\tau) = B_U^{\text{alloc}}(\tau) \cup B_i^{\text{alloc}}(\tau)$
  for (i, j) $i \in G$, $j \in R$ with lth highest $R_{\text{i,j}}(\tau)/T_{\text{i,j}}(\tau)$ **do**
    if $B_d^{\text{avail}}(\tau) > 0$ **then**
      $B_{i,j}^{\text{alloc}}(\tau) = \min(B_u^{\text{avail}}(\tau), B_i^{\text{need}}(\tau))$
      $B_d^{\text{avail}}(\tau) = B_d^{\text{avail}}(\tau) - B_{i,j}^{\text{alloc}}(\tau)$
      $B_D^{\text{alloc}}(\tau) = B_D^{\text{alloc}}(\tau) \cup B_{i,j}^{\text{alloc}}(\tau)$

Random Scheduler

A random scheduler is one where a random set of DERs are selected for uploading and downloading packets.

4.2.3 Ideal Scheduler

An ideal scheduler that communicates without any delays is used to compare the performances of all the other schedulers.

4.3 Performance Evaluation

This section describes the results in terms of AoI(T) and compares the performance of different schedulers on two microgrid test systems.

The DERs in both the systems are located in a rectangular region $l \times b$ with the BS at coordinates $(l/2, b/2)$. The path loss exponent γ is set as 3.76 per third generation partnership project (3GPP) urban path loss model [86]. The 5G network under consideration is using numerology $\mu = 0$. Test system I has 3 DERs while test system II has 28 DERs. The number of RBs in the UL and DL for test system I are $B_u = 2, B_d = 3$ and for test system II, they are $B_u = 10, B_d = 20$. The number of RBs needed to completely transmit a single packet for DER i, i.e., B_i, is randomly varied between 1 and 3. These values are summarized in Table 4.2. The channels, traffic generation and RB allocation are modeled as described in Section 4.1. The communication parameters used in the simulation are shown in Table 4.2.

The two test systems employ distributed control of DERs. The analysis is carried out in the dq-frame of reference [9]. For set point changes, V_{oq} is set to zero, and changes are applied to V_{od}. A metric called aggregate tracking error (ATE) is used to measure the system performance under different schedulers. It is defined as

$$\text{ATE} = \sum_{t=\text{start of disturbance}}^{\text{steady state}} \left| V_{od} - V_{sp} \right|. \tag{4.7}$$

The ATE for a scheduler is then normalized with respect to the ATE of an ideal scheduler. This is called the normalized aggregate tracking error (NATE) and is given as

$$\text{NATE} = \text{ATE}_{\text{scheduler}}/\text{ATE}_{\text{ideal}}. \tag{4.8}$$

4.3.1 Test System I

The first test system considered is the IEEE 34-bus distribution system as shown in Fig. 4.1. It operates in the grid-connected mode with a system base voltage of 24.9 kV. Three DERs operating in voltage control mode are added to the system. The DERs are modeled as a

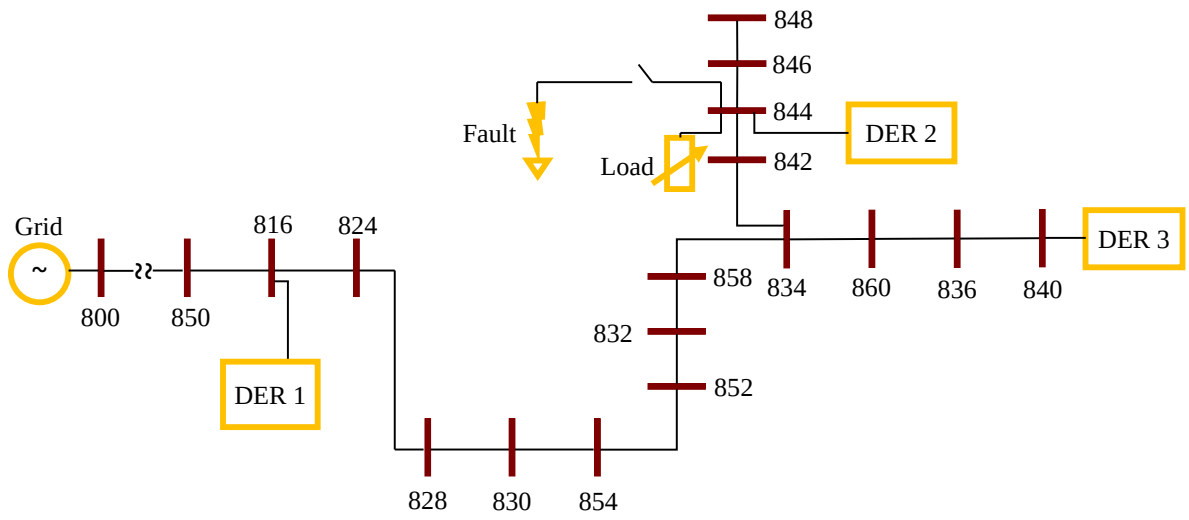

Figure 4.1: IEEE 34-bus test feeder with 3 DERs. Loads are not shown.

voltage-sourced converter (VSC) unit behind an LCL filter ($L = 1.8$ mH and $C = 100$ uF). The DERs communicate with each under distributed control. The adjacency matrix A is

$$A = \begin{bmatrix} 0 & 1 & 1 \\ 1 & 0 & 1 \\ 1 & 1 & 0 \end{bmatrix}. \tag{4.9}$$

Set Point Change in Output Voltage of a DER

The d-component of the output voltage set point of DER 2 is changed from 1.00 pu to 1.10 pu at $t = 0.1$ s, while V_{oq} is set to zero. The response under different schedulers is shown in Fig. 4.2. Table 4.3 shows the NATE values. It can be seen that MAD and MAF schedulers have lower NATE values compared with non-AoI schedulers. Compared with an ideal scheduler, there is a 21% and 28% increase in the NATE value for MAD and MAF schedulers. RR has an increased NATE of 53%, and the PF scheduler has an increased NATE of 80%. Random scheduler has the worst performance with an increased NATE of

Table 4.2: Communication Parameters used in simulation (developed in collaboration with Wireless@VT and submitted in [3])

Parameter	**Value**
Deployment region $l \times b$	1000m $\times$ 1000m
Transmission power $p^u_{\tau,\mathrm{f}}$	40 dBm [87]
Noise power σ_o	10^{-10} W
Path loss exponent γ	3.76 [86]
Channel	Rayleigh fading channel
CSI error variance σ_e^2	0.01 [86]
Traffic model	Generate at will
5G numerology μ	0
Number of DERs N	3, 28
Number of RBs in uplink B_u	2, 10
Number of RBs in downlink B_d	3, 20
RBs needed by ith DER B_i^{need}	[1,3] $\forall i \in G$
BS location	$(l/2, b/2)$

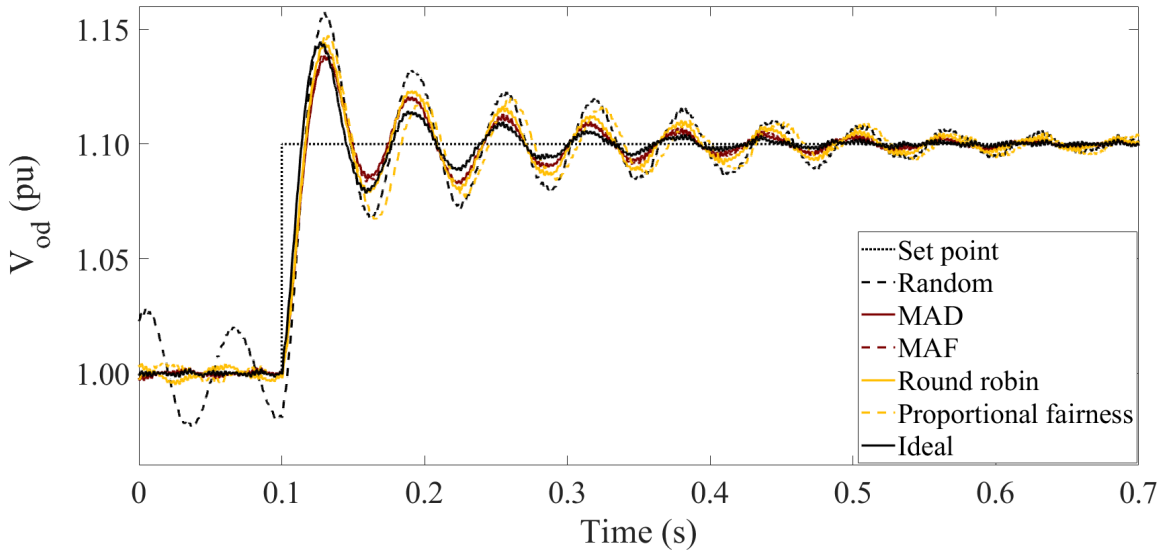

Figure 4.2: IEEE 34-bus system response of DER 2 to a step change in voltage set point from 1.00 pu to 1.10 pu at $t = 0.1$ s under different schedulers.

116% compared with the ideal scheduler.

Table 4.3: Normalized Aggregate tracking errors (NATE) for different schedulers (IEEE 34-bus distribution system)

Scheduler	**Normalized aggregate tracking error for different disturbances**		
	Voltage set point change	**Three-phase fault**	**Change in active load**
Ideal	1	1	1
MAD	1.21	1.19	1.22
MAF	1.28	1.26	1.26
Round robin	1.53	1.29	1.37
Proportional fairness	1.80	1.44	1.43
Random	2.16	1.89	2.01

Three-Phase to Ground Fault

A three-phase ABC-G fault is simulated at $t = 0.05$ s for 0.03 s at bus 844. The system response under different schedulers is shown in Fig. 4.3. It can be seen that AoI-aware schedulers have lower NATE values compared with non-AoI aware schedulers. MAD has a 19% higher NATE compared to the ideal scheduler. The RR scheduler has a 29% higher NATE compared with the ideal scheduler, while the random scheduler has a 89% higher NATE. The NATE values are shown in Table 4.3.

Change in Real Power of the Load

The real power of the load connected to bus 844 is changed from 1 MW to 20 MW at $t = 0.1$ s. The system response under different schedulers is shown in Fig. 4.4. From Table 4.3, it is seen that AoI-aware schedulers have a lower NATE values compared with non-AoI aware schedulers. RR and PF have a 12.29% and 17.2% higher NATE compared with MAD. Random scheduler has a 64.7% higher NATE compared with MAD.

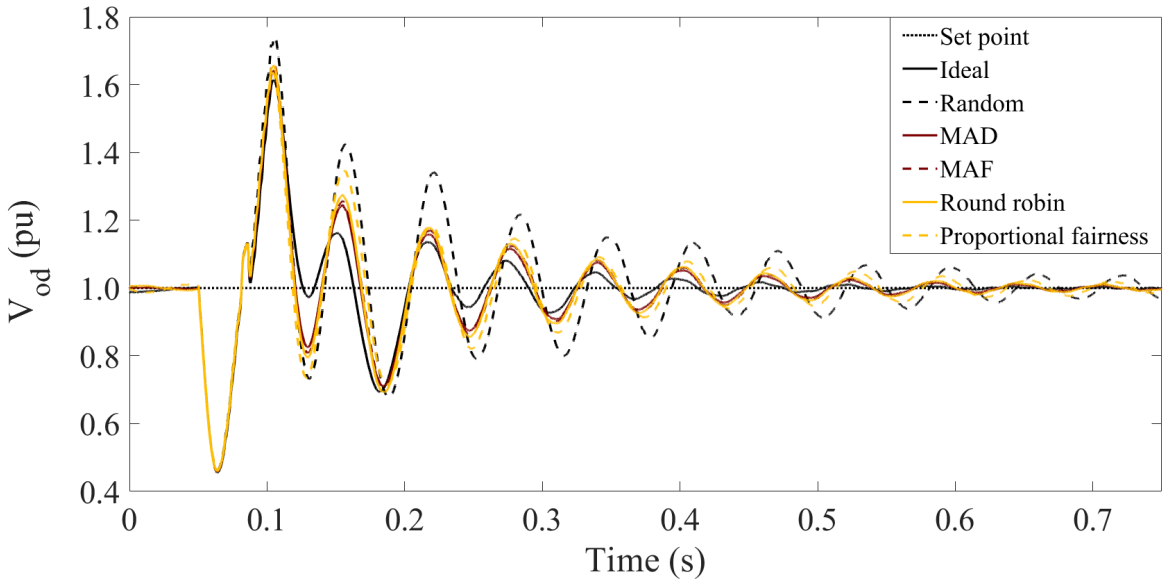

Figure 4.3: IEEE 34-bus system response to a ABC-G fault applied at bus 844 at $t = 0.05$ s for 0.03 s under different schedulers.

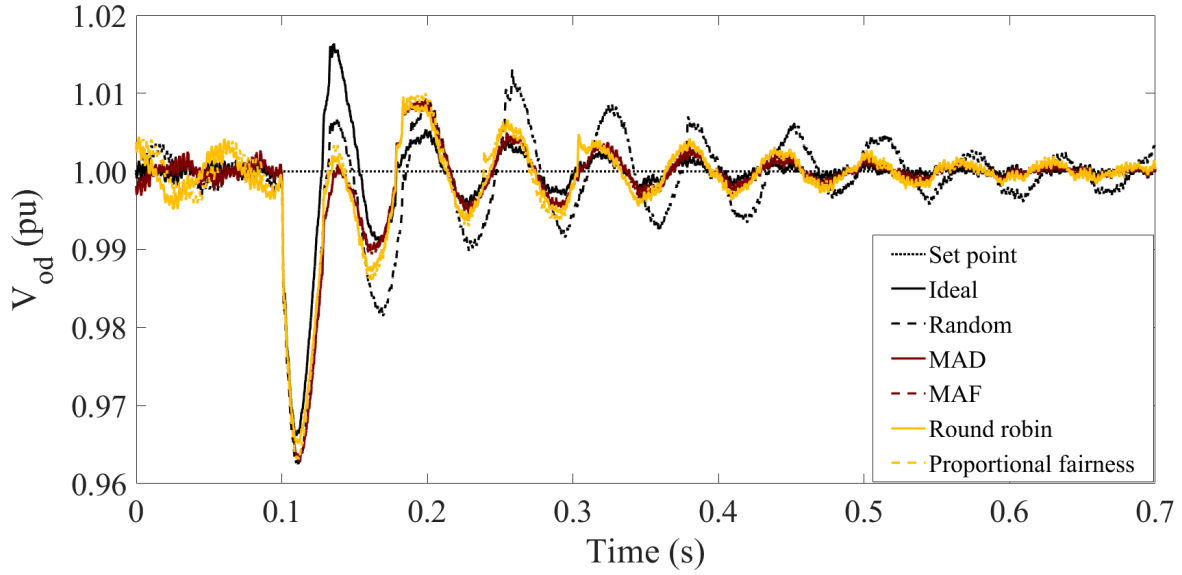

Figure 4.4: IEEE 34-bus system response to a change in real power of the load at bus 844 from 1 MW to 20 MW at $t = 0.1$ s under different schedulers.

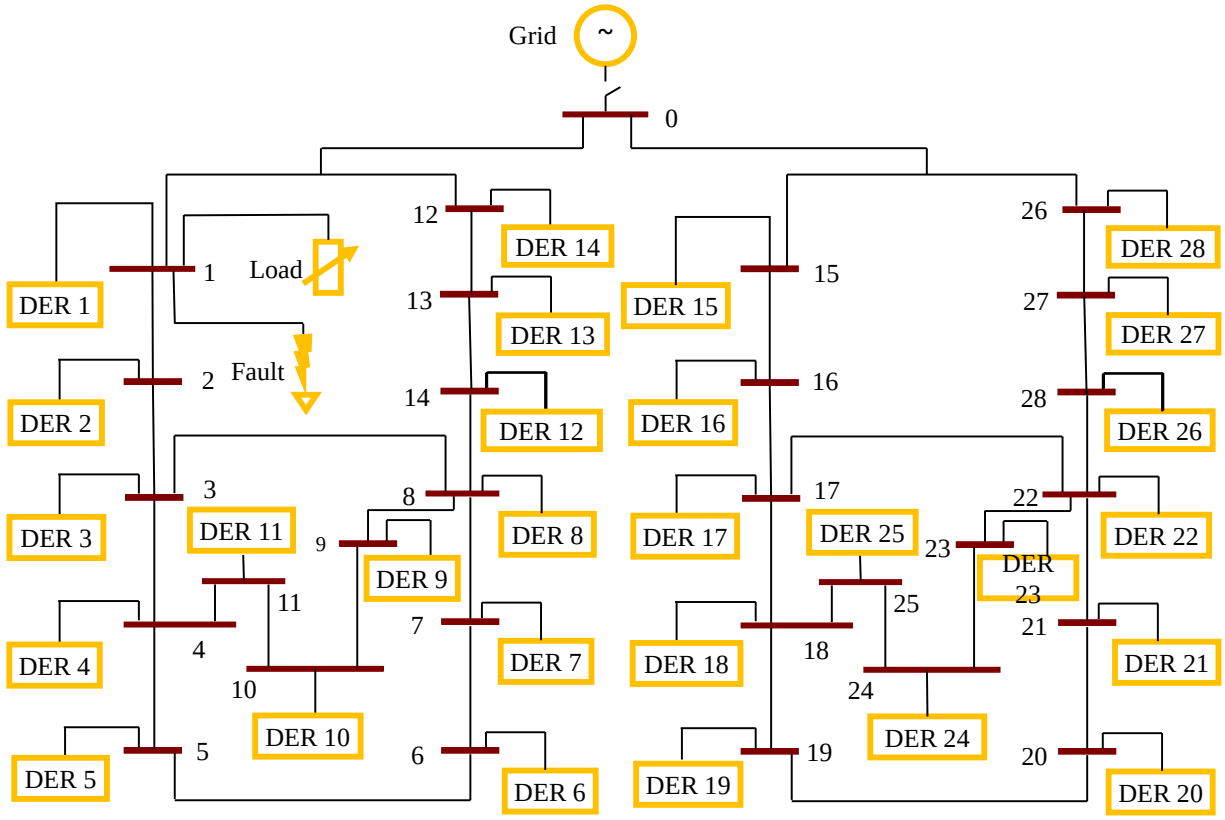

Figure 4.5: CIGRE distribution system with 28 DERs. Loads are not shown.

4.3.2 Test System II

The second test system considered is the CIGRE distribution system as shown in Fig. 4.5. It operates in the islanded mode with a system base voltage of 0.48 kV. The analysis is carried out in the dq-frame of reference. 28 DERs are augmented to the system. The DERs (rated 6 MVA) are modeled as a VSC unit behind an LCL filter ($L = 7.33$ uH and $C = 1.38$ mF). Each DER communicates with two other DERs near it under the distributed control objective. The interconnections are

DER 1 communicates with DER 2 and DER 14.

DER 14 communicates with DER 13 and DER 1.

Table 4.4: Normalized aggregate tracking errors (NATE) for different schedulers (CIGRE distribution system)

Scheduler	**Normalized aggregate tracking error for different disturbances**		
	Voltage set point change	**Three-phase fault**	**Change in active load**
Ideal	1	1	1
MAD	1.015	1.188	1.015
MAF	1.016	1.193	1.031
Round robin	1.023	1.220	1.038
Proportional fairness	1.029	1.226	1.043
Random	1.085	1.230	1.068

DER 15 communicates with DER 16 and DER 28.

DER 28 communicates with DER 27 and DER 15.

For $i \neq 1, 14, 15, 28$:

DER i communicates with DER $i-1$ and DER $i+1$.

The performance analysis under different disturbances is shown below.

Set Point Change in Output Voltage of a DER

The d-component of the output voltage set point of DER 1 is changed from 1.00 pu to 1.05 pu at $t = 0.1$ s, while V_{oq} is set to zero. The response under different schedulers is shown in Fig. 4.6. Table 4.4 shows the NATE values. It can be seen that MAD and MAF schedulers have lower NATE values compared with non-AoI schedulers. Compared with an ideal scheduler, there is a 1.5% and 1.6% increase in NATE for MAD and MAF schedulers. RR has an increased NATE of 2.3%, and the PF scheduler has an increased NATE of 2.9%. Random scheduler has the worst performance with an increased NATE of 8.5% compared with the ideal scheduler.

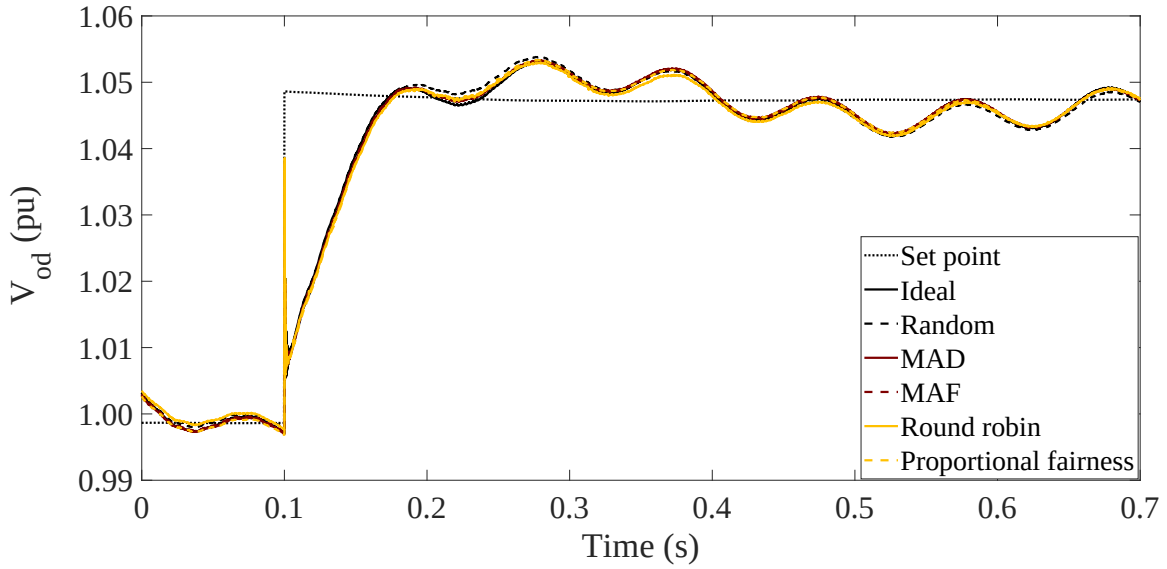

Figure 4.6: CIGRE system response of DER 1 to a step change in voltage set point from 1.00 pu to 1.05 pu at $t = 0.1$ s under different schedulers.

Three-Phase to Ground Fault

A three-phase ABC-G fault is simulated at $t = 0.1$ s for 0.03 s at bus 1. The response under different schedulers is shown in Fig. 4.7. It can be seen that AoI-aware schedulers have lower NATE values compared with non-AoI aware schedulers. MAD has a 19% higher NATE compared to the ideal scheduler. The RR scheduler has a 22% higher NATE compared with the ideal scheduler, while the random scheduler has a 23% higher NATE. The NATE values for all the schedulers is shown in Table 4.4.

Change in Real Power of the Load

The real power of the load connected to bus 1 is changed from 4.5 MW to 0.5 MW at $t = 0.1$ s. The response under different schedulers is shown in Fig. 4.8. Table 4.4 shows the NATE values for the different schedulers. It can be seen that MAD and MAF schedulers

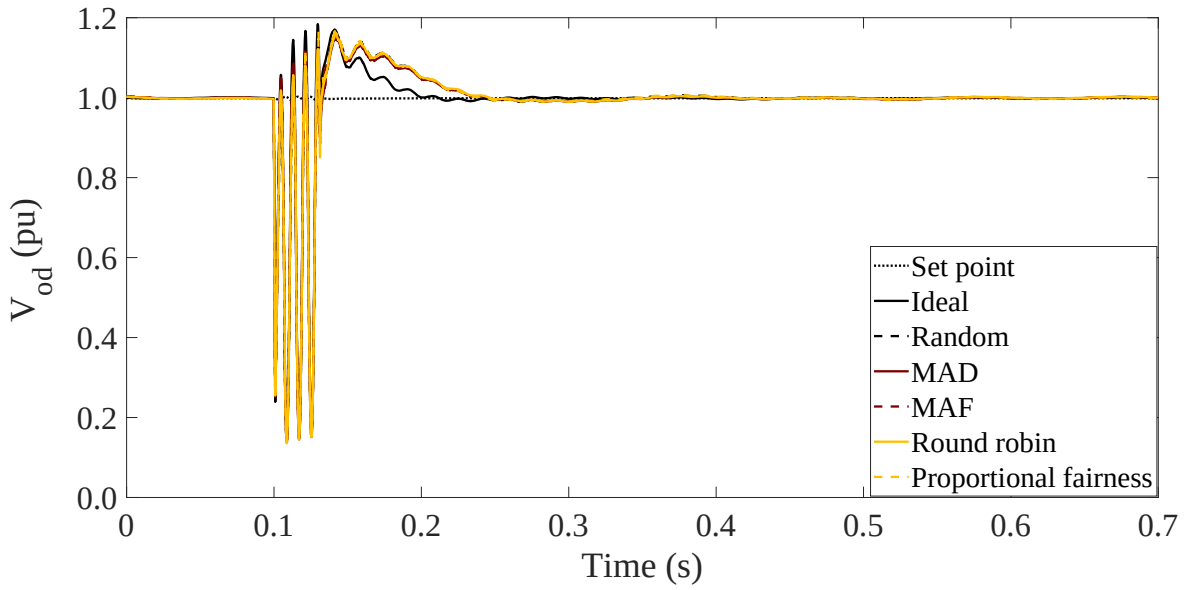

Figure 4.7: CIGRE system response to a ABC-G fault applied at bus 1 at $t = 0.1$ s for 0.03 s under different schedulers.

have lower NATE compared with other schedulers. RR and PF have a 2.26% and 2.76% higher NATE compared with MAD. Random scheduler has a 5.22% higher NATE compared with MAD.

Table 4.5 show the AoI(T) for the IEEE 34-bus system and CIGRE system. It can be seen that the AoI based schedulers outperform the non AoI based schedulers. This is because the AoI based schedulers (MAD and MAF) base their scheduling decisions explicitly on

Table 4.5: Age of Information (AoI(T)) at the destination DERs for the test cases

Schedulers	**IEEE 34-bus distribution system (ms)**	**CIGRE distribution system (ms)**
MAD	23992.01	215932.00
MAF	33402.91	232698.74
Round Robin	36696.97	326647.82
Proportional Fairness	47939.47	433371.46
Random	59873.52	514520.33

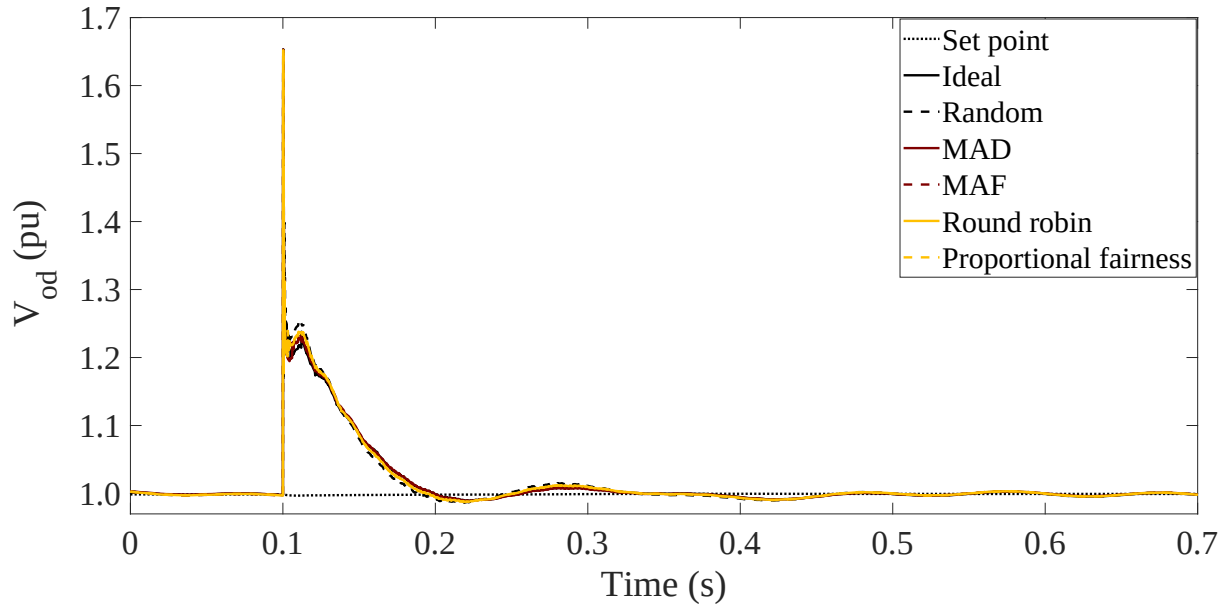

Figure 4.8: CIGRE system response to a change in real power of the load at bus 1 from 4.5 MW to 0.5 MW at $t = 0.1$ s under different schedulers.

AoI. MAD performs better than MAF, and this has also been observed in UAV-assisted internet of things (IoT) networks [88], where a UAV acts as a relay between IoT devices and a BS. This is because MAD leads to the maximum reduction in AoI at both the BS and the destination DERs [89]. Between the non-AoI schedulers, RR performs better than PF. RR has been shown to have better delay and throughput performance than PF [85, 90]. As the PF scheduler focuses on achieving fairness between all the DERs, it prioritize DERs with better channel conditions [85] which affects the AoI for DERs with bad channels condition resulting in the degradation of overall AoI.

Chapter 5

Conclusions

The contributions of this thesis are as follows:

- In this work, the effects of 5G scheduling in distributed control of microgrids have been investigated. Results from the test cases considered show that the grid is able to track the set point changes and handle transients in the presence of a 5G network.
- The thesis also compares the performance of AoI-aware 5G schedulers against non–AoI-aware 5G schedulers. The AoI based schedulers achieve better information freshness, which improves the microgrid performance. This implies that information freshness should be taken into consideration when designing 5G communication networks.

5G provides better bandwidth, throughput, and overall performance in comparison with other wireless technologies. Wired communication methods do not support plug and play operation as well as wireless methods do. With integration of more devices needing communication capabilities in the power system, this becomes a major drawback. Hence 5G is a suitable and viable solution for different power system applications.

The future research direction for this work can be summarized as follows:

- Extending 5G to other power system applications including protection.
- Adding physical device IDs and IP addresses to the DERs in the power system to incorporate encryption for cybersecurity purposes.

Bibliography

[1] R. Iyer, B. Choudhury, V. K. Shah, and A. Mehrizi-Sani, "Power systems performance under 5G radio access network in a co-simulation environment," *accepted in IEEE International Symposium on Industrial Electronics (ISIE)*, 2021.

[2] M. Kuzlu, M. Pipattanasomporn, and S. Rahman, "Communication network requirements for major smart grid applications in HAN, NAN and WAN," *Computer Networks*, vol. 67, pp. 74–88, 2014. [Online]. Available: https://www.sciencedirect.com/science/article/pii/S1389128614001431

[3] B. Choudhury, R. Iyer, A. Mehrizi-Sani, V. K. Shah, and J. Reed, "Design and analysis of age-optimal 5G schedulers for distributed control of microgrids," *IEEE Systems Journal*, Sep. 2021, submitted for review.

[4] D. Ton and M. Smith, "The U.S. department of energy's microgrid initiative," *The Electricity Journal*, vol. 25, p. 84–94, Oct. 2012.

[5] P. Bonanomi, "Phase angle measurements with synchronized clocks-principle and applications," *IEEE Transactions on Power Apparatus and Systems*, vol. PAS-100, no. 12, pp. 5036–5043, 1981.

[6] "Diving Into The Differences Between AC Microgrids And DC Microgrids," https://www.veckta.com/2021/05/27/the-differences-between-ac-microgrids-and-dc-microgrids/, (Accessed on 05/27/2021).

[7] H. Karimi, H. Nikkhajoei, and R. Iravani, "Control of an electronically-coupled distributed resource unit subsequent to an islanding event," in *2008 IEEE Power and*

Energy Society General Meeting - Conversion and Delivery of Electrical Energy in the 21st Century, 2008.

[8] K. Ahmed, M. Seyedmahmoudian, S. Mekhilef, N. M. Mubarak, and A. Stojcevski, "A review on primary and secondary controls of inverter-interfaced microgrid," *Journal of Modern Power Systems and Clean Energy*, pp. 1–17, 2020.

[9] F. Blaabjerg, R. Teodorescu, M. Liserre, and A. Timbus, "Overview of control and grid synchronization for distributed power generation systems," *IEEE Trans. Ind. Electron*, vol. 53, no. 5, pp. 1398–1409, Oct. 2006.

[10] M. Fakhari Moghaddam Arani and Y. A.-R. I. Mohamed, "Cooperative control of wind power generator and electric vehicles for microgrid primary frequency regulation," *IEEE Transactions on Smart Grid*, vol. 9, no. 6, pp. 5677–5686, 2018.

[11] Jiann-FuhChen and C.-L. Chu, "Combination voltage-controlled and current-controlled pwm inverters for parallel operation of UPS," in *Proceedings of IECON '93 - 19th Annual Conference of IEEE Industrial Electronics*, 1993, pp. 1111–1116 vol.2.

[12] M. A. Mahmud, M. J. Hossain, H. R. Pota, and A. M. T. Oo, "Robust nonlinear distributed controller design for active and reactive power sharing in islanded microgrids," *IEEE Transactions on Energy Conversion*, vol. 29, no. 4, pp. 893–903, 2014.

[13] M. Yazdanian and A. Mehrizi-Sani, "Distributed control techniques in microgrids," *IEEE Transactions on Smart Grid*, vol. 5, no. 6, pp. 2901–2909, 2014.

[14] B. Marinescu and H. Bourles, "Robust predictive control for the flexible coordinated secondary voltage control of large-scale power systems," *IEEE Transactions on Power Systems*, vol. 14, no. 4, pp. 1262–1268, 1999.

[15] Y. Wang, T. L. Nguyen, Y. Xu, Z. Li, Q.-T. Tran, and R. Caire, "Cyber-physical design and implementation of distributed event-triggered secondary control in islanded microgrids," *IEEE Transactions on Industry Applications*, vol. 55, no. 6, pp. 5631–5642, 2019.

[16] S. Peyghami, H. Mokhtari, P. C. Loh, P. Davari, and F. Blaabjerg, "Distributed primary and secondary power sharing in a droop-controlled LVDC microgrid with merged AC and DC characteristics," *IEEE Transactions on Smart Grid*, vol. 9, no. 3, pp. 2284–2294, 2018.

[17] S. Moayedi and A. Davoudi, "Distributed tertiary control of DC microgrid clusters," *IEEE Transactions on Power Electronics*, vol. 31, no. 2, pp. 1717–1733, 2016.

[18] F. Valenciaga and P. F. Puleston, "High-order sliding control for a wind energy conversion system based on a permanent magnet synchronous generator," *IEEE Transactions on Energy Conversion*, vol. 23, no. 3, pp. 860–867, 2008.

[19] M. Mehdi, C.-H. Kim, and M. Saad, "Robust centralized control for DC islanded microgrid considering communication network delay," *IEEE Access*, vol. 8, pp. 77 765–77 778, 2020.

[20] M. M. A. Abdelaziz, M. F. Shaaban, H. E. Farag, and E. F. El-Saadany, "A multistage centralized control scheme for islanded microgrids with PEVs," *IEEE Transactions on Sustainable Energy*, vol. 5, no. 3, pp. 927–937, 2014.

[21] N. L. Díaz, A. C. Luna, J. C. Vasquez, and J. M. Guerrero, "Centralized control architecture for coordination of distributed renewable generation and energy storage in islanded AC microgrids," *IEEE Transactions on Power Electronics*, vol. 32, no. 7, pp. 5202–5213, 2017.

[22] A. Colet-Subirachs, A. Ruiz-Alvarez, O. Gomis-Bellmunt, F. Alvarez-Cuevas-Figuerola, and A. Sudria-Andreu, "Centralized and distributed active and reactive power control of a utility connected microgrid using IEC 61850," *IEEE Systems Journal*, vol. 6, no. 1, pp. 58–67, 2012.

[23] I. V. Prasanna, D. Srinivasan, and S. K. Panda, "Design, analysis and implementation of a four-tier centralized control architecture for intelligent operation of grid-connected microgrids," in *2016 IEEE International Conference on Power Electronics, Drives and Energy Systems (PEDES)*, 2016.

[24] Y. Sabri, N. El Kamoun, and F. Lakrami, "A survey: Centralized, decentralized, and distributed control scheme in smart grid systems," in *2019 7th Mediterranean Congress of Telecommunications (CMT)*, 2019.

[25] R. Anderson, "Final report on the blackout in the united states and canada: Causes and recommendations final report on the blackout in the united states and canada: Causes and recommendations," Aug. 2004.

[26] G. Lou, W. Gu, J. Wang, W. Sheng, and L. Sun, "Optimal design for distributed secondary voltage control in islanded microgrids: Communication topology and controller," *IEEE Transactions on Power Systems*, vol. 34, no. 2, pp. 968–981, Mar. 2019.

[27] J. Llanos, D. E. Olivares, J. W. Simpson-Porco, M. Kazerani, and D. Sáez, "A novel distributed control strategy for optimal dispatch of isolated microgrids considering congestion," *IEEE Transactions on Smart Grid*, vol. 10, no. 6, pp. 6595–6606, Nov. 2019.

[28] M. H. Syed, E. Guillo-Sansano, D. Wang, A. Mehrizi-Sani, Y. Wang, G. M. Burt, and Y. Xu, "Coordinated set point modulation of DERs for dynamically robust set point tracking as a virtual power plant," *IEEE Transactions on Power Systems*, Oct. 2020, submitted for review.

[29] Z. Zhang and M.-Y. Chow, "Convergence analysis of the incremental cost consensus algorithm under different communication network topologies in a smart grid," *IEEE Transactions on Power Systems*, vol. 27, no. 4, pp. 1761–1768, Nov. 2012.

[30] S. T. Cady, A. D. Domínguez-García, and C. N. Hadjicostis, "A distributed generation control architecture for islanded AC microgrids," *IEEE Transactions on Control Systems Technology*, vol. 23, no. 5, pp. 1717–1735, 2015.

[31] V. Nasirian, S. Moayedi, A. Davoudi, and F. L. Lewis, "Distributed cooperative control of DC microgrids," *IEEE Transactions on Power Electronics*, vol. 30, no. 4, pp. 2288–2303, 2015.

[32] S. Trip, M. Cucuzzella, X. Cheng, and J. Scherpen, "Distributed averaging control for voltage regulation and current sharing in DC microgrids," *IEEE Control Systems Letters*, vol. 3, no. 1, pp. 174–179, 2019.

[33] E. Espina, J. Llanos, C. Burgos-Mellado, R. Cárdenas-Dobson, M. Martínez-Gómez, and D. Sáez, "Distributed control strategies for microgrids: An overview," *IEEE Access*, vol. 8, pp. 193 412–193 448, 2020.

[34] R. Zhang and B. Hredzak, "Distributed finite-time multiagent control for DC microgrids with time delays," *IEEE Transactions on Smart Grid*, vol. 10, no. 3, pp. 2692–2701, 2019.

[35] M. A. Shahab, B. Mozafari, S. Soleymani, N. M. Dehkordi, H. M. Shourkaei, and J. M. Guerrero, "Distributed consensus-based fault tolerant control of islanded microgrids," *IEEE Transactions on Smart Grid*, vol. 11, no. 1, pp. 37–47, 2020.

[36] S. F. Bush, S. Goel, and G. Simard, "Ieee vision for smart grid communications: 2030

and beyond roadmap," *IEEE Vision for Smart Grid Communications: 2030 and Beyond Roadmap*, pp. 1–19, 2013.

[37] N. L. Díaz, J. C. Vasquez, and J. M. Guerrero, "A communication-less distributed control architecture for islanded microgrids with renewable generation and storage," *IEEE Transactions on Power Electronics*, vol. 33, no. 3, pp. 1922–1939, 2018.

[38] I. Serban, "A control strategy for microgrids: Seamless transfer based on a leading inverter with supercapacitor energy storage system," *Applied Energy*, vol. 221, pp. 490–507, 2018. [Online]. Available: https://www.sciencedirect.com/science/article/pii/S0306261918304604

[39] S. Marzal, R. A. Salas Puente, R. González-Medina, G. Garcera, and E. Figueres, "Current challenges and future trends in the field of communication architectures for microgrids," *Renewable and Sustainable Energy Reviews*, vol. 82, 11 2017.

[40] H. Shahinzadeh, A.-s. Mirhedayati, M. Shaneh, H. Nafisi, G. B. Gharehpetian, and J. Moradi, "Role of joint 5G-IoT framework for smart grid interoperability enhancement," in *2020 15th International Conference on Protection and Automation of Power Systems (IPAPS)*, 2020, pp. 12–18.

[41] S. Ghosh, C. K. Chanda, and J. K. Das, "A comprehensive survey on communication technologies for a grid connected microgrid system," in *2021 International Conference on Artificial Intelligence and Smart Systems (ICAIS)*, 2021, pp. 1525–1528.

[42] M. Elkashlan, T. Q. Duong, and H.-H. Chen, "Millimeter-wave communications for 5G: fundamentals: Part I [guest editorial]," *IEEE Communications Magazine*, vol. 52, no. 9, pp. 52–54, 2014.

[43] L. Lu, G. Y. Li, A. L. Swindlehurst, A. Ashikhmin, and R. Zhang, "An overview of

massive MIMO: Benefits and challenges," *IEEE Journal of Selected Topics in Signal Processing*, vol. 8, no. 5, pp. 742–758, 2014.

[44] C.-X. Wang, F. Haider, X. Gao, X.-H. You, Y. Yang, D. Yuan, H. M. Aggoune, H. Haas, S. Fletcher, and E. Hepsaydir, "Cellular architecture and key technologies for 5G wireless communication networks," *IEEE Communications Magazine*, vol. 52, no. 2, pp. 122–130, 2014.

[45] K. Hosseini, J. Hoydis, S. ten Brink, and M. Debbah, "Massive MIMO and small cells: How to densify heterogeneous networks," in *2013 IEEE International Conference on Communications (ICC)*, 2013, pp. 5442–5447.

[46] S. Wu, H. Wang, and C.-H. Youn, "Visible light communications for 5G wireless networking systems: from fixed to mobile communications," *IEEE Network*, vol. 28, no. 6, pp. 41–45, 2014.

[47] X. Ge, S. Tu, G. Mao, C.-X. Wang, and T. Han, "5G ultra-dense cellular networks," *IEEE Wireless Communications*, vol. 23, no. 1, pp. 72–79, 2016.

[48] "How 5G SDN Will Bolster Networks," https://www.sdxcentral.com/5g/definitions/5g-sdn/, (Accessed on 10/31/2017).

[49] N. Aitken, "How 5G Differs From Previous Wireless Network Generations," https://whatphone.com.au/guide/how-5G-differs-from-previous-wireless-network-generations.

[50] N. Surantha, N. Sutisna, Y. Nagao, and H. Ochi, "SoC design with HW/SW co-design methodology for wireless communication system," in *2017 17th International Symposium on Communications and Information Technologies (ISCIT)*, 2017.

[51] V. Garg and T. Rappaport, "Wireless network evolution: 2G to 3G," 2001.

[52] H. Hui, Y. Ding, Q. Shi, F. Li, Y. Song, and J. Yan, "5G network-based internet of things for demand response in smart grid: A survey on application potential," *Applied Energy*, vol. 257, p. 113972, 2020. [Online]. Available: https://www.sciencedirect.com/science/article/pii/S0306261919316599

[53] G. Bedi, G. K. Venayagamoorthy, R. Singh, R. R. Brooks, and K.-C. Wang, "Review of internet of things (IoT) in electric power and energy systems," *IEEE Internet of Things Journal*, vol. 5, no. 2, pp. 847–870, 2018.

[54] X. Huang and S. Wang, "Aggregation points planning in smart grid communication system," *IEEE Communications Letters*, vol. 19, no. 8, pp. 1315–1318, 2015.

[55] M. Garau, M. Anedda, C. Desogus, E. Ghiani, M. Murroni, and G. Celli, "A 5G cellular technology for distributed monitoring and control in smart grid," in *2017 IEEE International Symposium on Broadband Multimedia Systems and Broadcasting (BMSB)*, 2017.

[56] X. Chen, W. Ni, T. Chen, I. B. Collings, X. Wang, and G. B. Giannakis, "Real-time energy trading and future planning for fifth generation wireless communications," *IEEE Wireless Communications*, vol. 24, no. 4, pp. 24–30, 2017.

[57] M. Garau, M. Anedda, C. Desogus, E. Ghiani, M. Murroni, and G. Celli, "A 5G cellular technology for distributed monitoring and control in smart grid," in *2017 IEEE international symposium on broadband multimedia systems and broadcasting (BMSB)*. IEEE, Jun. 2017.

[58] S. Sofana Reka, T. Dragičević, P. Siano, and S. Prabaharan, "Future generation 5G wireless networks for smart grid: A comprehensive review," *Energies*, vol. 12, no. 11, p. 2140, 2019.

[59] G. Wikström, J. Torsner, J. Kronander, O. Al-Saadeh, F. Chernogorov, G. Bag, J. Neander, K. Landernäs, and P. Hovila, "Wireless protection of power grids over a 5G network," in *2019 IEEE PES GTD Grand International Conference and Exposition Asia (GTD Asia)*, Mar 2019, pp. 976–981.

[60] M. Yazdanian and A. Mehrizi-Sani, "Distributed control techniques in microgrids," *IEEE Transactions on Smart Grid*, vol. 5, no. 6, pp. 2901–2909, 2014.

[61] M. Prodanovic and T. C. Green, "High-quality power generation through distributed control of a power park microgrid," *IEEE Transactions on Industrial Electronics*, vol. 53, no. 5, pp. 1471–1482, Oct. 2006.

[62] "3GPP TS 38.306. User Equipment (UE) radio access capabilities. version 15.3.0 Rel 15."

[63] "3GPP TS 38.214. Physical layer procedures for data version. 15.3.0 Rel 15."

[64] R. Dilli, "Analysis of 5G Wireless Systems in FR1 and FR2 Frequency Bands," in *2020 2nd International Conference on Innovative Mechanisms for Industry Applications (ICIMIA)*, Mar. 2020, pp. 767–772.

[65] "5g nr modulation and coding scheme – modulation and code rate," https://www.techplayon.com/5g-nr-modulation-and-coding-scheme-modulation-and-code-rate/.

[66] https://www.verizon.com/info/definitions/bandwidth/.

[67] "What is a numerology," https://apistraining.com/5g-numerology/.

[68] "NR Scheduling Performance Evaluation - MATLAB & Simulink," https://www.mathworks.com/help/5g/ug/nr-tdd-symbol-based-scheduling-performance-evaluation.html, (Accessed on 01/11/2021).

[69] "Ericsson Mobility Report November 2016," https://www.ericsson.com/en/mobility-report/reports, (Accessed on 12/06/2020).

[70] A. Mehrizi-Sani and R. Iravani, "Online set point modulation to enhance microgrid dynamic response: Theoretical foundation," *IEEE Transactions on Power Systems*, vol. 27, no. 4, pp. 2167–2174, Nov. 2012.

[71] Y. Xu and W. Wang, "Wireless mesh network in smart grid: Modeling and analysis for time critical communications," *IEEE Transactions on Wireless Communications*, vol. 12, no. 7, pp. 3360–3371, Jul. 2013.

[72] M. Tanaka, D. Umehara, M. Morikura, N. Otsuki, and T. Sugiyama, "New throughput analysis of long-distance IEEE 802.11 wireless communication system for smart grid," in *Proc. IEEE Int. Conf. on Smart Grid Comm. (SmartGridComm)*, Oct. 2011, pp. 90–95.

[73] O. Vondrouš, P. Macejko, T. Hégr, and Z. Kocur, "Testing methodology for performance evaluation of communication systems for smart grid," in *Proc. 2nd International Conference on IGBSG.*, Jun. 2016.

[74] B. Choudhury, V. K. Shah, A. Dayal, and J. H. Reed, "Experimental analysis of safety application reliability in v2v networks," in *Proc. IEEE 91st Vehicular Technology Conference (VTC-Spring).*, May. 2020.

[75] B. Choudhury, V. K. Shah, A. Dayal, and J. Reed, "Joint age of information and self risk assessment for safer 802.11 p based v2v networks," *IEEE Conference on Computer Communications (INFOCOM)*, 2021.

[76] Y. Wang, S. Wu, J. Jiao, W. Wu, Y. Wang, and Q. Zhang, "Age-optimal transmission

policy with HARQ for freshness-critical vehicular status updates in space-air-ground integrated networks," *IEEE Internet of Things Journal*, Dec. 2020.

[77] M. Chen, Y. Xiao, Q. Li, and K.-C. Chen, "Minimizing Age-of-Information for Fog Computing-supported Vehicular Networks with Deep Q-learning," in *Proc. IEEE International Conference on Communications (ICC)*, Jun. 2020.

[78] A. Cao, C. Shen, J. Zong, and T.-H. Chang, "Peak age-of-information minimization of UAV-aided relay transmission," in *IEEE International Conference on Communications Workshops (ICC Workshops)*, Jun. 2020.

[79] M. Samir, C. Assi, S. Sharafeddine, and A. Ghrayeb, "Online altitude control and scheduling policy for minimizing AoI in UAV-assisted IoT wireless networks," *IEEE Transactions on Mobile Computing*, Dec. 2020.

[80] J. Hu, H. Zhang, L. Song, R. Schober, and H. V. Poor, "Cooperative internet of UAVs: Distributed trajectory design by multi-agent deep reinforcement learning," *IEEE Transactions on Communications*, vol. 68, no. 11, pp. 6807–6821, Nov. 2020.

[81] M. Yi, X. Wang, J. Liu, Y. Zhang, and B. Bai, "Deep reinforcement learning for fresh data collection in UAV-assisted IoT networks," in *IEEE Conference on Computer Communications (INFOCOM WKSHPS)*, 2020, pp. 716–721.

[82] M. A. Abd-Elmagid, A. Ferdowsi, H. S. Dhillon, and W. Saad, "Deep reinforcement learning for minimizing age-of-information in UAV-assisted networks," in *IEEE Global Communications Conference (GLOBECOM)*, Dec. 2019.

[83] "5G NR Physical channels and modulation, Release 15," 3GPP TS 38.211 version 15.3.0, Sophia Antipolis, France, Oct. 2018.

[84] C. J. Katila, C. Buratti, M. D. Abrignani, and R. Verdone, "Neighbors-aware proportional fair scheduling for future wireless networks with mixed MAC protocols," *EURASIP Journal on Wireless Communications and Networking*, vol. 2017, no. 1, May. 2017.

[85] C. F. Müller, G. Galaviz, Á. G. Andrade, I. Kaiser, and W. Fengler, "Evaluation of scheduling algorithms for 5G mobile systems," in *Computer Science and Engineering—Theory and Applications*. Springer, Feb. 2018, pp. 213–233.

[86] P. K. Korrai, E. Lagunas, A. Bandi, S. K. Sharma, and S. Chatzinotas, "Joint power and resource block allocation for mixed-numerology-based 5G downlink under imperfect CSI," *IEEE Open Journal of the Communications Society*, vol. 1, pp. 1583–1601, Oct. 2020.

[87] P. Korrai, E. Lagunas, S. K. Sharma, S. Chatzinotas, A. Bandi, and B. Ottersten, "A RAN resource slicing mechanism for multiplexing of eMBB and URLLC services in OFDMA based 5G wireless networks," *IEEE Access*, vol. 8, pp. 45 674–45 688, Mar. 2020.

[88] B. Choudhury, V. K. Shah, A. Ferdowsi, J. H. Reed, and Y. T. Hou, "AoI-minimizing scheduling in UAV-relayed IoT networks," *accepted in IEEE Conference on Mobile Ad-Hoc and Smart Systems (MASS)*, 2021.

[89] J. Song, D. Gunduz, and W. Choi, "Optimal scheduling policy for minimizing age of information with a relay," *arXiv preprint arXiv:2009.02716*, 2020.

[90] D. Perdana, A. N. Sanyoto, and Y. G. Bisono, "Performance evaluation and comparison of scheduling algorithms on 5G networks using network simulator," *International Journal of Computers Communications & Control*, vol. 14, no. 4, pp. 530–539, Aug. 2019.